Individual chain dynamics of a polyethylene melt undergoing steady shear flow

M. H. Nafar Sefiddashti, B. J. Edwards,[a] and B. Khomami

Materials Research and Innovation Laboratory (MRAIL), Department of Chemical and Biomolecular Engineering, University of Tennessee, Knoxville, Tennessee 37996

(Received 8 September 2014; final revision received 14 November 2014; published 9 December 2014)

Synopsis

Individual molecule dynamics have been shown to influence significantly the bulk rheological and microstructural properties of short-chain, unentangled, linear polyethylene liquids undergoing high strain-rate flows. The objective of this work was to extend this analysis to a linear polyethylene composed of macromolecules of a much greater length and entanglement density; i.e., a liquid consisting of $C_{400}H_{802}$ molecules, with approximately ten kinks per chain at equilibrium, as calculated by the Z1 code of Kröger [Comput. Phys. Commun. **168**, 209–232 (2005)]. To achieve this, we performed nonequilibrium molecular dynamics (NEMD) simulations of a model system using the well-established potential model of Siepmann *et al*. [Nature **365**, 330–332 (1993)] for a wide range of Weissenberg numbers (Wi) under steady shear flow. A recent study by Baig *et al*. [Macromolecules **43**, 6886–6902 (2010)] examined this same system using NEMD simulations, but focused on the bulk rheological and microstructural properties as calculated from ensemble averages of the chains comprising the macromolecular liquids. In so doing, some key features of the system dynamics were not fully elucidated, which this article aims to highlight. Specifically, it was found that this polyethylene liquid displays multiple timescales associated with not only the decorrelation of the end-to-end vector (commonly related to the Rouse time or disengagement time, depending on the entanglement density of the liquid), but also ones associated with the retraction and rotation cycles of the individual molecules. Furthermore, when accounting for these individual chain dynamics, the "longest" relaxation time of the system was higher by a factor of 1.7, independent of shear rate, when calculated self-consistently due to the coupling of relaxation modes. Brownian dynamics (BD) simulations were also performed on an analogous free-draining bead-rod chain model to compare the rotation and retraction dynamics of a single chain in dilute solution with individual molecular motions in the melt. These BD simulations revealed that the dynamics of the free-draining chain are qualitatively and quantitatively similar to those of the individual chains comprising the polyethylene melt at strain rates in excess of $Wi \approx 50$, implying a possible breakdown of reptation theory in the high shear limit. An examination of the bulk-average properties revealed the effects of the chain rotation and retraction cycles upon commonly modeled microstructural properties, such as the distribution function of the chain end-to-end vector and the entanglement number density. © *2015 The Society of Rheology*.
[http://dx.doi.org/10.1122/1.4903498]

[a]Author to whom correspondence should be addressed; electronic mail: bje@utk.edu

I. INTRODUCTION

The description of fast flows of macromolecular fluids has proven to be a difficult challenge for rheologists. Many theories were proposed during the 20th century in attempts to explain the rheological and microstructural responses of these complex liquids under flow, but each invariably diverged from experiment at high strain rates, regardless of their degree of success in the linear and weakly nonlinear viscoelastic flow regimes (i.e., at low to intermediate values of the strain rate relative to a characteristic relaxation time of the fluid). Many conjectures have been proposed for these discrepancies at high strain rates, such as the failure of closure approximations, mode coupling effects, a strain-rate dependent relaxation time, and many others, depending on the nature of the specific model under consideration. The most basic reason for this near universal failure of rheological models for high strain-rate flow is simply that all of the relevant physical processes have not been incorporated self-consistently into the mathematical constitutive equations that are presumed to describe the fluid response.

In the 21st century, reptation theory is widely considered to be the gold standard of contemporary rheological ideology. The basic premise of this theory, originating from an idea of de Gennes (1971), is that a macromolecular chain experiences snakelike diffusion through contorted tubes formed by the surrounding chainlike molecules. The physical constraints of these tubes mandate that the diffusional motion parallel to the polymer backbone is greater than the motion perpendicular to it. This simple physical picture was encoded into a descriptive theory of polymer dynamics under flow by Doi and Edwards (1986) a decade later, and extensively developed over the next three decades—see McLeish (2002) for a relatively recent exposition of the state of reptation theory. Today it is almost universally viewed as the most fundamental and inherently accurate description of entangled polymeric liquid microstructural and dynamical responses to external stimuli.

In spite of the wide acceptance and application of reptation theory, it possesses some well-known deficiencies, most of which are primarily evident under the imposition of high strain-rate flows. Whereas experiment and atomistic simulations have verified most of the dynamical behavior predicted by reptation theory under equilibrium (no-flow) conditions, and also for low and intermediate strain-rate flows, the consistency of this theory with experimental data for high strain-rate flows has been incomplete and the applicable physics is still not fully understood.

Recent evidence suggests that a flow-induced disentanglement of polymer macromolecules can occur at high strain rates in steady shearing flow. This reduction in interchain constraints leads to the onset of individual molecular retraction and rotation cycles, which occur within roughly oriented tubelike structures composed of the highly extended surrounding chain molecules. This new phenomenon has been observed in nonequilibrium molecular dynamics simulations of molten polyethylenes in the unentangled and moderately entangled molecular-weight regimes (i.e.; polyethylenes up to $C_{400}H_{802}$) [Kim *et al*. (2008a); Kim *et al*. (2008b); Kim *et al*. (2009, 2010); Kim *et al*. (2011); Baig *et al*. (2010)]. This unexpected observation from atomistic simulations can possibly explain the difficulties that manifest in reptation theory for high strain-rate flows, as elucidated in this article.

II. BACKGROUND

Observations of the motions of individual chain molecules are crucial to further development and refinement of rheological and topological models of the dynamics of

polymeric liquids. Most past modeling efforts have been aimed at the description of the evolution of bulk-averaged quantities, such as the conformation or stress tensors, under the influence of an applied external flow field [Bird *et al*. (1987a); Bird *et al*. (1987b)]. These theories are applicable to chain liquids at low field strength, but their descriptions of the rheological behavior tend to break down once the field strength drives the fluid substantially beyond the linear viscoelastic regime. Unfortunately, the averaging procedure implies a substantial reduction in the number of degrees of freedom of the molecular-scale description, resulting in characteristic evolution equations for variables (such as the conformation tensor or the extra stress tensor) that change on macroscopic length and time scales but ignore the atomistic-scale dynamics. Consequently, any information that is present on microscopic timescales is effectively removed from the final evolution equations that describe the dynamical response of the chain liquid. This readily explains why these bulk-averaged theories often break down in the nonlinear viscoelastic regime where the timescales of the flow can become smaller than those associated with the time evolution of the macroscopic variables. (Note that as strain rate is increased, its reciprocal, associated with the characteristic timescale of the flow, decreases.) Many examples of the failure of bulk-averaged models, especially at high strain rates, were discussed by Larson (1988).

A large number of attempts have been made to extend the validity of dynamical equations for entangled polymers into the nonlinear viscoelastic regime [Bird *et al*. (1987b); Larson (1988)]. The most popular model is the reptation-based theory of Doi and Edwards (1986), wherein a generic chain is assumed to undergo snakelike motion within a contorted tube formed by neighboring chains. Consequently, motion along the chain contour is much less restrained than motion perpendicular to it. A characteristic timescale is assigned to this motion, τ_d, which is called the "reptation" or "disengagement" timescale; conceptually, this is the time required for the chain to disengage from its original tube. This timescale is generally some multiple of the fluid's Rouse time, τ_R, under quiescent (no-flow) conditions. Although the most comprehensive versions of reptation-based theories perform well at low shear rates $(\dot{\gamma} < 1/\tau_d)$ [Larson (1999)], and have recently attained success at intermediate shear rates $(1/\tau_d < \dot{\gamma} < 1/\tau_R)$ [Mhetar and Archer (2000); Islam *et al*. (2003)], they still struggle to describe completely the rheology and topology of entangled polymeric liquids at high shear rates where the associated timescales become relatively small $(1/\tau_R < \dot{\gamma})$ [Teixeira *et al*. (2007)].

Until recently, light scattering and birefringence experiments were the primary means for analyzing the orientational and configurational changes of polymer chains undergoing flow; however, these types of experimentation are unable to resolve configurational changes of individual polymer chains. Consequently, these measurement techniques were restricted to examining bulk fluid properties and could not distinguish between phenomena that occur over disparate length and time scales; however, this does not imply that the dynamics of individual chain molecules do not affect the observed birefringence and light scattering patterns.

Relatively recent direct visualization of individual polymer chains using video microscopy offered the possibility to explore the motions of individual chain molecules undergoing flow [Smith and Chu (1998); Smith *et al*. (1999); LeDuc *et al*. (1999); Teixeira *et al*. (2005), Teixeira *et al*. (2007); Schroeder *et al*. (2005); Robertson and Smith (2007); Harasim *et al*. (2013)]. These initial studies have seriously called into question many of the assumptions used to model polymer flow dynamics. Smith *et al*. (1999) and LeDuc *et al*. (1999) simultaneously examined dilute solutions of DNA, in which the dynamics of individual, labeled chains were visualized under shear in the flow-vorticity plane using video microscopy. These results demonstrated that the flexible polymer chains

experienced both deformation and tumbling under shear, as a function of the Weissenberg number ($Wi = \tau_R \dot{\gamma}$). Schroeder *et al*. (2005), Teixeira *et al*. (2005), and Teixeira *et al*. (2007) visualized and tracked individual configurational changes of fluorescently labeled DNA solutions under steady shear flow in the flow-gradient plane for concentrations ranging from dilute to highly entangled. These experiments again demonstrated the tumbling and stretching dynamics of individual chains, which depended on both Wi and concentration, but the evidence was more direct since the visualization was carried out in the flow-gradient plane. They also demonstrated a *quasiperiodic* tumbling of the individual DNA molecules in dilute solution at high Wi, with a characteristic frequency for this rotation that scaled sublinearly with shear rate as $Wi^{0.62}$. For concentrated DNA solutions, two distinct timescales were observed: The first associated with the chain retraction dynamics (the short timescale), and the second possibly related to the dynamics of constraint release and contour length fluctuations (the long timescale). The probability distribution of chain extension broadened dramatically at high Wi from its approximately Gaussian shape at low Wi, which is not typical of preaveraged bulk rheological theory. Robertson and Smith (2007) used optical tweezers to measure the intermolecular forces acting on a single DNA chain as exerted by the surrounding entangled molecules and found three distinct timescales: The short timescale was determined as close to the theoretical value of the Rouse time, the long timescale was associated with the disengagement time of reptation theory, and the intermediate timescale was speculated to be a second reptative process that was correlated with the dynamics of the effective reptation tube under shear. Harasim *et al*. (2013) examined dilute suspensions of semiflexible actin filaments and observed distinct chain-end retraction and tumbling cycles of individual molecules, book-ended by periods of maximum chain extension.

Despite the numerous successes of single-chain microscopy to date, experimentation alone cannot resolve all of the outstanding issues that perplex rheologists at high Wi. The primary limitation of these experiments is the small number of molecules that can be effectively tracked simultaneously, which is especially true of dense polymer melts. Atomistic or coarse-grained mesoscopic simulation of entangled polymeric liquids offers a complementary perspective of individual chain dynamics under flow. In particular, slip-link simulations with full-chain spatial coupling have been successful in accurately predicting the linear and nonlinear shear rheology as well as single-chain dynamics of fluids composed of entangled polymeric chains [Schieber *et al*. (2007); Dambal *et al*. (2009)]; however, the accuracy of the predictions, particularly for very fast flows, i.e., $(1/\tau_R < \dot{\gamma})$, strongly depends on the assumed constraint renewal/release frequency [Kushwaha and Shaqfeh (2011)]. Clearly, at high deformation rates the constraint renewal/release frequency should depend on the deformation rate. This critical modification to the state-of-the-art slip-link models requires detailed understanding of individual macromolecule dynamics at high deformation rates. The experimental difficulty associated with tracking a sufficiently large number of single molecules in highly entangled polymeric liquids makes nonequilibrium molecular dynamics (NEMD) simulations a suitable method for determination of this critical information.

Nonequilibrium molecular dynamics is a common technique used to study flows of chain molecules comprised of atomistically detailed particles or coarse-grained models, such as bead-spring chains where each bead represents a center of drag resistance to the surrounding flow and the spring represents a statistical segment of the atomistic chain. Most NEMD flow simulations to date have focused on the determination of bulk rheological and structural properties, whether performed for either atomistic [Mavrantzas and Theodorou (1998); Moore *et al*. (2000); Mavrantzas and Öttinger (2002); Baig *et al*. (2006); Kim *et al*. (2008a); Baig and Mavrantzas (2009)] or coarse-grained [Kröger *et al*.

(1993); Öttinger (1996); Doyle *et al*. (1997); Kröger and Hess (2000); Schieber *et al*. (2007); Venkataramani *et al*. (2008); Dambal *et al*. (2009); Kushwaha and Shaqfeh (2011)] liquids. Although much new insight concerning the relationships between flow kinematics, material properties, and microstructure has been gained from these studies, this focus on bulk behavior at macroscopic length and time scales has resulted in overlooking key microscopic information concerning the molecular-scale origin of the bulk rheological and structural properties [Kim *et al*. (2009, 2010); Kim *et al*. (2011)], as described below.

The primary advantage of NEMD simulation of an atomistically detailed polymer chain over experiment is that every chain within the sample can be examined individually, not just those which were optically labeled and under view in the experimental apparatus. This allows much more detailed information to be gleaned from the simulation with respect to the experiment, as statistically meaningful correlations can be established via ensemble averaging of the dynamical behavior of each individual chain. Also, simulations are readily amenable to topological analysis, extending equilibrium properties such as tube diameter, primitive path length, and number of entanglements to nonequilibrium flow situations [Kim *et al*. (2008b)]. Certainly, bulk-averaged properties, such as the conformation and stress tensors, can still be calculated, but also with the ability to examine the effects of short timescale individual chain dynamics upon them. Ultimately, more and better information at the microscopic scale should lead to better rheological and microstructural models of polymeric liquids under flow. Indeed, recent simulations studies wherein the short timescale phenomena have been examined and analyzed carefully have already led to new insight regarding the effects of molecular-scale, segmental motions on the dynamical flow response, as well as models that incorporate these phenomena [Schieber *et al*. (2007); Dambal *et al*. (2009); Kim *et al*. (2010); Kim *et al*. (2011); Kushwaha and Shaqfeh (2011)]; these recent insights are described in the succeeding paragraphs.

Six years ago, Kim *et al*. (2008a), Kim *et al*. (2008b), and Kim *et al*. (2009) noticed an apparent anomaly in the steady-shear behavior of a short-chain polyethylene ($C_{78}H_{158}$) melt in a NEMD simulation; i.e., the probability distribution of the end-to-end vector, $\mathbf{R}$, which connects the two end units of the carbon chain, became bimodal at high values of *Wi*. At low values of *Wi*, the distribution was essentially Gaussian with the peak centered at approximately its equilibrium value of $|\mathbf{R}|$, as expected, and this distribution gradually widened and the peak shifted to higher values of $|\mathbf{R}|$ at intermediate *Wi* with the increasing extension of the polymer molecules under flow, also as expected. At high *Wi*, however, two peaks emerged, one associated with the continued deformation of the molecules, which approached the maximum extension of the chains at high *Wi*, and a second one that appeared at values of $|\mathbf{R}|$ that were actually smaller than the equilibrium value [see Fig. 3 of Kim *et al*. (2009)]. Even more puzzling was the additional fact that the macroscopic, ensemble-averaged conformation tensor displayed the expected behavior at all values of *Wi* [Kim *et al*. (2011)]. This is an important point since a typical flow birefringence or small-angle light scattering experiment indirectly measures the conformation tensor and not the distribution of $|\mathbf{R}|$. However, using the conformation tensor calculated in the simulations, which very accurately resembles the experimentally determined one, produces a unimodal distribution when one examines its Eigenvalues and Eigenvectors. In other words, a bulk-flow experiment cannot recognize other than the usual unimodal distribution and is blind to the possibility of a multimodal distribution at high *Wi*; hence an apparent example of the complementary use of experiment and atomistic simulations. As a consequence, the presence of a bimodal distribution could have gone unnoticed for many years.

The problem with using the conformation tensor as a descriptor of the microstructural state of a polymeric liquid is that it is a long-time ensemble average over the chainlike molecules. Therefore, the short timescale dynamics of the chains are effectively averaged out over an extended period of time. Furthermore, performing the ensemble averaging over all chains tends to weight the highly extended chains more than those at the low end of the $|\mathbf{R}|$ spectrum, thus emphasizing the "stretch peak" of the bimodal distribution at high Wi.

To resolve the apparent anomaly of the bimodal distribution, it was ultimately necessary to study the dynamical behavior of the ensemble of chains by looking at each chain individually—something that cannot be done experimentally, especially in these dense melts. In doing so, a new and unexpected insight was gained into the dynamic behavior of these macromolecular liquids at short timescales, and how this behavior affects macroscopic bulk-flow properties. To understand the origin of the peak at low values of $|\mathbf{R}|$, it is necessary to examine the dynamics of individual chains as they undergo steady shear flow. Kim *et al*. (2009) demonstrated that the cause of the bimodal distribution was associated with the individual chains experiencing periods of high extension followed by short excursions of rotational tumbling where the ends of a polymer chain passed each other very closely, with an associated flip in the orientational angle. Consequently, it became apparent that the low $|\mathbf{R}|$ peak of the bimodal distribution at high Wi was due to the time-averaging of these fast quasiperiodic tumbling cycles, whereas the high $|\mathbf{R}|$ peak quantified the highly extended chain configurations, which persisted over longer timescales than the relatively rapid rotation.

Ideally, the periodic nature of these tumbling events could be quantified by calculating appropriate autocorrelation and cross-correlation functions of the end-to-end vector. Therefore, Kim *et al*. (2009) examined the time correlation functions of the various components of $|\mathbf{R}|$, and found that at low values of Wi, these correlations all decayed monotonically, as expected, with a characteristic relaxation time that corresponded to the Rouse time of this unentangled $C_{78}H_{158}$ liquid at equilibrium. However, at large Wi, these correlations developed a damped oscillatory behavior that could be quantified by a power spectral density calculation and characterized by two timescales, as defined by the equation

$$\langle R_\alpha(t)\, R_\beta(t+\tau)\rangle = A \exp\left(-t/\tau_{conv}\right) \cos\left(2\pi t/\tau_{\alpha\beta}\right), \tag{1}$$

where A is a constant, $\tau_{\alpha\beta}$ is a characteristic timescale associated with the rate of rotation, and τ_{conv} is a convective timescale of configurational decorrelation that corresponds to the Rouse time when Wi lies in the range [0,1]. The characteristic times resulting from Eq. (1) showed that the rotational timescales decreased as the frequency of the rotations increased with increasing Wi. It was noted that the critical Wi where a breakdown of the stress-optical rule occurred in prior simulations [Baig *et al*. (2007)] corresponded fairly well to the critical Wi where the onset of rotational motion became evident [Kim *et al*. (2009, 2010)]. The primary conclusion drawn from these prior results is that chain ends undergo quasiperiodic fluctuations into the flow-vorticity plane during which they can begin to experience anisotropic diffusion down the axis of "tubes" formed by the surrounding, highly oriented chains.

It is worth noting that an analogous type of periodic rotational and diffusional motion has been observed in simulations before [Aust *et al*. (1999); Aust *et al*. (2002); Doyle *et al*. (1997); Venkataramani *et al*. (2008)]; these simulations have all invoked mesoscopic models of bead-spring or bead-rod chains suspended at dilute concentrations in low molecular-weight solvents where the model chains were free to maintain Jeffreys'-type

tumbling orbits and stretch-recoil cycles without experiencing interference from surrounding chains. Edberg *et al*. (1987) also found evidence of molecular rotation and stretching in NEMD simulations of small chain liquids (*n*-butane and *n*-decane); however, the simulations of an analogous periodic behavior in the dense melts on relatively large *n*-alkane chains, as described above, were quite unexpected.

Kim *et al*. (2008b) also examined the topological characteristics of the $C_{78}H_{158}$ liquid and noticed that the least primitive path of the chain molecules was highly dependent on *Wi*, experiencing an initial increase at low values of *Wi*, an apparent maximum corresponding to the critical flow strength where chain rotation became significant, and a subsequent decrease as the molecular tumbling cycles produced more tightly coiled chain configurations on average, ultimately resulting in primitive paths that were shorter than those of the equilibrium system. Furthermore, the number of entanglements per chain was shown to decrease steadily with increasing *Wi* due to the uncoiling effect of the highly elongated chain configurations that comprise the stretch peak of the bimodal distribution at any particular instant. The effective reptation tube diameter initially increased at low *Wi*, followed by an apparent maximum and subsequent decrease with increasing *Wi*. Once again, the maximum in the primitive path was clearly associated with the critical value of *Wi* where chain rotation and retraction became a significant component of the overall system dynamical response.

Kim *et al*. (2011) used the simulation results described above to develop and test a stochastic model based on the ansatz of anisotropic chain diffusion through tubes formed by surrounding, highly aligned chains. The polymer chains were mesoscopically modeled as bead-spring chains, with a finitely extensible nonlinear elastic force law applied to the springs. The basic principle in the bead-spring model is that chain segments composed of many atomistic backbone units can be modeled collectively as a series of springs, each of which characterizes the resultant forces of all the atomic constituents, with each spring bounded between two beads that represent conceptual centers of frictional resistance with the surrounding medium. Kim *et al*. (2011) applied a force balance over the bead-spring chain to derive an anisotropic diffusion model under the primary hypothesis that at high strain rates, when significant disentanglement occurs, the underlying dynamics of the polymer chains resemble very closely the behavior that is observed for semi-dilute and concentrated polymer solutions, as in visualization experiments [Smith and Chu (1998); Smith *et al*. (1999); LeDuc *et al*. (1999); Teixeira *et al*. (2005); Teixeira *et al*. (2007); Schroeder *et al*. (2005); Robertson and Smith (2007)]. This being the case, it is reasonable to assume that mesoscopic models, such as the one described above, will provide an accurate description of the individual molecular dynamics. Consequently, each chain is surrounded by a mean-field of highly aligned chains that form an effective "tube" through which a single chain can experience anisotropic diffusion that is enhanced in the direction of the tube axis and inhibited perpendicular to the tube axis. In principle, this allows chains in a mesoscopic Brownian dynamics (BD) simulation to recoil and rotate similarly to the chains in the atomistic NEMD simulations.

The model described above was able to fit the standard rheological characteristic functions (viscosity, first and second normal stress coefficients) and average molecular extensions (magnitude of the end-to-end vector, etc.) of the atomistic NEMD simulations quantitatively using a single adjustable parameter with a universal value. This value (0.6) was slightly greater than the value of this ratio (0.5) derived by Doi and Edwards (1986) for rigid rodlike molecules, which makes sense based on the stated hypothesis. More importantly, however, was the fact that the model was able to describe quantitatively the bimodal distribution observed in the NEMD simulations as well as the characteristic timescales of the rotational motion [Kim *et al*. (2011)].

Although the phenomenon of molecular rotation described above is very interesting, its relevance to real-world polymer dynamics can be questioned since the simulated liquid was composed of fairly short-chain polyethylenes with only 78 carbon units. Macromolecules of this length are only faintly entangled, with an average of about one entanglement per chain at equilibrium, whereas fully entangled polymer melts are generally considered to average 20–30 entanglements, and often many more. Consequently, it is highly possible that increasing the number of entanglements per chain, not to mention simply increasing the length of the chains, might hinder the type of anisotropic molecular diffusion that was observed in the short-chain simulations. Therefore, longer chains were examined in subsequent studies ($C_{400}H_{802}$) by Baig *et al*. (2010), where the chains average about five entanglements per chain under quiescent conditions; hence the macromolecules can be viewed as moderately entangled from a reptation perspective. These authors performed an extensive suite of NEMD simulations at *Wi* values ranging from 0 to 21 600 and calculated many bulk fluid properties via ensemble averaging, such as the end-to-end vector distribution, rheological characteristic functions, the conformation tensor, number of entanglements, least primitive path, molecular energies, and reptation tube diameters. Essentially all of these results were qualitatively similar to those from the $C_{78}H_{158}$ NEMD simulations, as described above. These results were rather surprising in that all of the unusual behavior observed in the unentangled $C_{78}H_{158}$ simulations carried over into the much longer moderately entangled $C_{400}H_{802}$ simulations. However, the lack of focus on the dynamics of the individual macromolecules comprising the fluid left a gap in the understanding of this moderately entangled polymeric liquid, which the present contribution aims to fill. Specifically, the relationships between the bulk-averaged system properties and the onset of chain rotation and retraction, as well as the associated coupled timescales, were not elucidated in the prior work, and will be examined more critically herein. Some of the results of Baig *et al*. (2010) will be reproduced in this article to retain continuity, but the reader is referred to the cited paper for a complete presentation of the prior work.

III. SIMULATION METHODOLOGY

A. Nonequilibrium molecular dynamics

The system studied in this work is a monodisperse $C_{400}H_{802}$ linear polyethylene melt. The simulation conditions were adopted from a previous work on $C_{400}H_{802}$ by Baig *et al*. (2010) in order to facilitate a comparison with their results. The rectangular simulation volume contained 198 $C_{400}H_{802}$ chains, subject to periodic boundary conditions on all sides of the box. The *NVT* simulations were performed at constant temperature (450 K) and constant density ($0.7640\,g/cm^3$) corresponding to a well-established experimental state point at atmospheric pressure. The dimensions of the simulation volume were 86.96 Å along the y (gradient) and z (neutral) directions and 318.8 Å along the x (flow) direction. As the flow is in the x direction, this box dimension was set considerably larger than the other two directions since under high shear the chains would stretch and orient at a small angle with respect to the x axis. The maximum possible extension of the chains, $|\mathbf{R}|_{max}$, is approximately 515 Å when all bond dihedral angles are in the trans-configuration while bond lengths and angles maintain their equilibrium values; therefore, 318.8 Å should be sufficient to minimize systems size effects that might occur during the high shear simulations where significant degrees of chain extension and orientation can be induced by the flow. An extended simulation box of dimensions ($516 \times 68.5 \times 68.5$ Å) was also examined at *Wi* values of 1060 and 10 000 to ensure that individual chains could

not extend through both ends of the simulation cell in the flow direction; results proved that all measured properties were statistically unchanged from the original simulation cell.

The simulation box comprised 79 200 united atoms making up the 198 chainlike molecules, which conformed to the Siepmann–Karaborni–Smit (SKS) united-atom potential model [Siepmann *et al*. (1993)] except that the rigid bond between adjacent atoms in the original model was replaced with a harmonic potential function; this is standard practice in molecular dynamics simulations as use of this potential model alleviates integration difficulties. The united-atom particles represent either -CH_3 or -CH_2- groups, depending on location along the chain. All intermolecular and intramolecular potential functions (bond-stretching, bond-bending, etc.) were the same as employed in many prior simulation studies [Moore *et al*. (2000); Baig *et al*. (2006); Baig *et al*. (2007); Baig *et al*. (2010); Baig and Mavrantzas (2009); Kim *et al*. (2008a); Kim *et al*. (2008b); Kim *et al*. (2009, 2010); Kim *et al*. (2011)], with the only exception being the bond-torsional potential

$$U_{tor}(\phi) = \sum_{m=0}^{3} a_m (\cos\phi)^m, \tag{2}$$

where the bond-torsional constants were $a_0/k_B = 1010\,K$, $a_1/k_B = -2019\,K$, $a_2/k_B = 136.4\,K$, and $a_3/k_B = 3165\,K$. Although Eq. (2) is the same as in the previous studies, the values of a_1/k_B and a_3/k_B have the opposite signs to those used in most prior work; this is because the program used in the present work defined the dihedral angle such that the trans-configuration is located at 180° rather than at 0°.

The p-SLLOD equations of motion were used to perform the NEMD simulations, which were maintained at a constant temperature of 450 K using a Nosé–Hoover thermostat [Nosé (1984); Hoover (1985); Evans and Morriss (1990); Edwards and Dressler (2001); Edwards *et al*. (2005, 2006); Baig *et al*. (2005)]. The full set of evolution equations for the system are can be found in several of the cited references. The upper limit of strain rates examined is believed to be below the threshold where thermostat artifacts begin to affect the system response [Travis *et al*. (1995); Baig *et al*. (2006)].

The equations of motion were implemented within the large-scale atomic/molecular massively parallel simulator (LAMMPS) environment. Boundary conditions were periodic at all box surfaces with a deforming simulation box in the x direction. The equations were integrated using the reversible reference system propagator algorithm, r-RESPA, with two different time steps. The long time step was 2.35 fs, which was used for the slowly varying nonbonded Lennard-Jones (LJ) interactions. The short time step was 0.47 fs (one-fifth of the long time step) for the rapidly varying forces including bond-bending, bond-stretching, and bond torsional interactions. The relaxation time of the thermostat was set equal to 0.235 ps in all simulations. Roughly the same range of shear rates was examined as in the study of Baig *et al*. (2010); i.e., $(4.59 \times 10^6\,\mathrm{s}^{-1} \leq \dot{\gamma} \leq 9.63 \times 10^{10}\,\mathrm{s}^{-1})$.

The topological analysis was performed using the Z1 code developed by Kröger (2005), which reduces atomistic configurations to a primitive path network in which the chains are not allowed to cross through each other as the algorithm simultaneously minimizes the contour length of each polymer molecule [Karayiannis and Kröger (2009)]. This method uses geometrical methods rather than dynamical algorithms to minimize the contour lengths of primitive paths in the most computationally efficient manner. The code further defines positions of kinks along the three-dimensional primitive path of each chain, which are assumed to be roughly proportional to the number of entanglements per chain. Results of the code can be used to interpret other important reptative parameters,

such as the effective tube diameter and entanglement strand length. The Z1 method has been compared with other topological analysis techniques by Shanbhag and Kröger (2007).

B. BD

BD simulations were also performed for a free-draining bead-rod chain to assess the similarities and differences between single-chain dynamical behavior in the $C_{400}H_{802}$ melt and an analogous chainlike macromolecule in dilute solution under shear. Simulations were performed using methods described elsewhere [Doyle *et al*. (1997); Somasi *et al*. (2002); Kim *et al*. (2010)]. The linear $C_{400}H_{802}$ macromolecule was modeled mesoscopically as a freely jointed chain of 32 beads separated by rigid rods 16.5 Å in length, as discussed in Sec. IV of this article.

The BD simulations assumed a sum of three external forces acting on the beads, which satisfied a conservation equation for each bead. These forces were the hydrodynamic drag force, as described by Stokesian friction acting on the beads, a constraint force, which maintains constant bond length (b) between adjacent beads, and a Brownian force that describes collisions between neighboring beads. The resulting set of evolution equations for the position vectors of the beads was solved using the iterative technique developed by Liu (1989), which has been proven to be optimal for this size of chains by Somasi *et al*. (2002).

The BD simulations were performed by matching the longest relaxation time of the bead-rod model to the equilibrium value of 231 ns, as extracted from the atomistic equilibrium simulation—see below for specific details. Equilibrium and flow properties were calculated using long-time ensemble averages of 1000 replicated chain systems.

IV. RESULTS AND DISCUSSION

A. Quiescent properties

Simulation data of the autocorrelation functions of the unit and scaled end-to-end vectors versus time of the $C_{400}H_{802}$ liquid under quiescent conditions are presented in Fig. 1. The autocorrelation function of the i-th chain unit end-to-end vector, as expressed in terms of the usual chain end-to-end vector, $\mathbf{u}_i = \mathbf{R}_i/|\mathbf{R}_i|$, is represented as $\langle \mathbf{u}_i(\tau) \cdot \mathbf{u}_i(\tau + t) \rangle$, where τ is an arbitrary reference time and the angular brackets denote an ensemble average over all of the 198 chains in the simulated liquid. The autocorrelation function of the scaled end-to-end vector is defined as $\langle \bar{\mathbf{R}}_i(\tau) \cdot \bar{\mathbf{R}}_i(\tau + t) \rangle$, where $\bar{\mathbf{R}}_i = \mathbf{R}_i/\langle R^2 \rangle^{1/2}$ is weighted with respect to the equilibrium value of $\langle R^2 \rangle = 8482$ Å^2 as determined from the simulation. Although the system relaxation times are usually developed in terms of correlation functions of either $\mathbf{R}_i$ or $\bar{\mathbf{R}}_i$, we chose here to primarily use $\mathbf{u}_i$, as did Baig *et al*. (2010). Our primary motivation for doing so is because the autocorrelation function of $\mathbf{u}_i$ weights each chain equally, rather than an unscaled end-to-end vector that weights highly extended chains with longer values of $|\mathbf{R}_i|$ more heavily than those with low extensions. This is important at the high values of Wi to be examined later where the end-to-end vector can be quite small due to frequent rotation and retraction cycles, which can reduce $|\mathbf{R}_i|$ to very small values, even less than the equilibrium value. We simulated the liquid dynamics for a system composed of 198 chains for 1200 ns, a factor of three higher than the timespan simulated by Baig *et al*. (2010), who used a simulation of 54 chain molecules for the quiescent case [Baig (personal communication)]; given the nature of a calculation of the correlation function, our data should therefore be inherently more accurate.

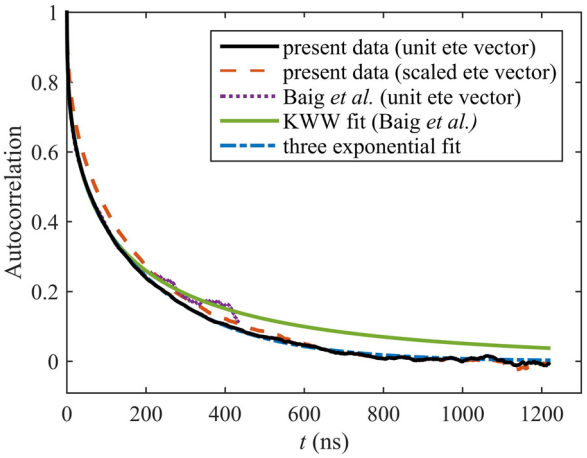

FIG. 1. Autocorrelation functions of $\langle \mathbf{u}_i(\tau) \cdot \mathbf{u}_i(\tau + t) \rangle$ and $\langle \bar{\mathbf{R}}_i(\tau) \cdot \bar{\mathbf{R}}_i(\tau + t) \rangle$ versus time under quiescent conditions. Data are presented for the present simulations as well as those of Baig *et al*. (2010). The fit to the unit end-to-end (ete) vector data set of the present work is given by a sum of three exponentials, whereas the fit to the data set of Baig *et al*. is via the KWW equation.

The time correlation functions for our equilibrium simulation and that of Baig *et al*. (2010) are presented in Fig. 1, where the latter data were generously shared with us by Dr. Baig (personal communication). The present data decay exponentially to zero over the long timespan of the simulation, whereas that of Baig *et al*. ends well short of total decay. Because of this, there is some degree of error evident in the final 200 ns of their data. Based on a fit of the Kohlrausch–Williamson–Watts (KWW) equation [Larson 1999],

$$\langle \mathbf{u}_i(\tau) \cdot \mathbf{u}_i(t + \tau) \rangle = A_K \exp\left[-\left(\frac{t}{\tau_K} \right)^{\beta_K} \right]. \tag{3}$$

Baig *et al*. estimated the longest system relaxation time to be 218 ns. In Eq. (3), τ is an arbitrary reference time and A_K, τ_K, and $\beta_K \in [0,1]$ are fitting parameters that allow an estimation of the longest system relaxation time. The KWW equation is thus a stretched exponential expression which allows a much better estimation of the longest relaxation time of the system when only a limited amount of simulation data are available. Using this expression, our estimate of the longest system relaxation time is 154 ns, which is significantly lower than that of Baig *et al*.; however, given the extensive amount of present data, there is no need to employ the KWW equation, and a sum of simple exponentials can be used to estimate multiple system relaxation times, not just the longest one. Sums of two and three exponentials gave very good fits to the data, and the relaxation times determined via a least-squares fit are presented in the first two columns of Table I. (The three-exponential fit is displayed in Fig. 1.) Based on the three-exponential fit, the relaxation times are calculated as 2.4, 28, and 231 ns. (Sums including additional exponential functions, containing four and five functions, respectively, gave longest relaxation times very near to 231 ns as well.) The longest of the these (231 ns) was used to calculate the values of *Wi* used in the shear flow simulations for the range of shear rates stated above; i.e., $Wi \in [1.06,\ 22\,250]$. Note that the value of the relaxation time obtained from a fit of the KWW equation (154 ns) drastically underestimates the actual longest relaxation time. Based upon the value of 218 ns, Baig *et al*. (2010) reportedly examined the range of

TABLE I. The three relaxation times calculated from the autocorrelation function of the unit end-to-end vector, $\mathbf{u}_i$, according to two and three-term series of exponential functions, segmental MSD data, and reptation theory.

Relaxation time	Two-exponential	Three-exponential	MSD	Theory
τ_e (ns)	—	2.4	2.6	5.1
τ_R (ns)	16	28	20	18
τ_d (ns)	225	231	279	273

$Wi \in [0.54,\ 21\,600]$; however, their value of the longest relaxation is sufficiently close to our value such that the shift in the simulated data when plotted against Wi should be negligible, enabling direct comparisons between our results and those of Baig *et al*.

Figure 1 also displays the correlation function $\langle \bar{\mathbf{R}}_i(\tau) \cdot \bar{\mathbf{R}}_i(\tau + t) \rangle$ of the scaled end-to-end vector. A fit of a sum of two exponentials to the data yields characteristic timescales of 18 and 228 ns, whereas a sum of three exponentials gives 2.9, 29, and 232 ns. Comparing these values with those of Table I, it is evident that these timescales are very close to those obtained from similar fits of the unit end-to-end vector autocorrelation. The scaled vector correlation is slightly higher than that of the unit vector, which is expected since the more highly extended chains are weighted more heavily in the scaled vector calculation, although this effect is fairly small at equilibrium since the probability of finding highly extended chains is very low. Most of the difference between the two sets of data manifests in the prefactors of the terms in the exponential summations, not in the characteristic timescales.

We hypothesize that the three relaxation times calculated using the unit end-to-end vector correlation function in Table I correspond to actual physical processes of the $C_{400}H_{802}$ liquid, as described by reptation theory. The smallest of these, 2.4 ns, corresponds to the entanglement time, τ_e, which is associated with the timescale for individual chain segments to feel the confining constraints of the tube formed from the surrounding chains. The intermediate timescale is associated with the Rouse time, τ_R, and the longest relaxation time is associated with the disengagement time, τ_d, which is the time required for the chain to escape from its initial tube. We can use deductions from reptation theory to justify this hypothesis, as discussed below.

According to reptation theory of a Gaussian chain [Doi and Edwards (1986)], the Rouse and disengagement timescales are governed by the expressions

$$\tau_R = \frac{\xi N^2 b^2}{3\pi^2 k_B T}, \tag{4}$$

$$\tau_d = \frac{1}{\pi^2} \frac{\xi N^3 b^4}{k_B T\, a^2}, \tag{5}$$

where ξ is the friction coefficient of the identical beads, N is the number of beads per chain (which is approximately the number of Kuhn steps for long chains), b is the Kuhn length, and a is the step length of the primitive chain or, equivalently, the tube diameter. The Kuhn length, as approximated by $b = \langle R^2 \rangle / |\mathbf{R}|_{\max}$, is determined directly from the simulation as 16.5 Å, based on the equilibrium $\langle R^2 \rangle^{1/2}$ value of 92.1 Å. This value is slightly larger than the 89.5 Å calculated by Baig *et al.* (2010); however, the two values are within the mutual error tolerances of each other. Hence the number of Kuhn segments is $31.29 \approx 31$. Defining the radius of gyration as R_g, the ensemble average $\langle R_g^2 \rangle = 1369$ Å^2.

The number of steps in a primitive chain, or the number of entanglements per chain, is defined as [Doi and Edwards (1986)]

$$Z = \frac{\langle L \rangle}{a} = \frac{Nb^2}{a^2}, \tag{6}$$

where Z is the number of entanglements per chain and $\langle L \rangle$ is the average primitive chain contour length, which was calculated using the Z1 code as 209 Å. The number of entanglements is given by the expression $Z = \langle L \rangle^2 / R^2$, where we have defined $R^2 \equiv Nb^2$. This will be assumed to be equivalent to $\langle R \rangle^2 = 8482$ Å^2. Accordingly, the number of entanglements is calculated using this expression as $Z = 5.15$, and hence the tube diameter is 40.6 Å from Eq. (6). This value of Z compares well with the experimental value of ≈4.9 reported by Fetters *et al.* (1999). Alternatively, a can be calculated according to $a = b(N_e)^{1/2}$, where $N_e = N/Z$ is the number of Kuhn steps per entanglement strand, which also gives 40.6 Å. These values compare well with the value of the step length of the primitive path, a_s, for the same $C_{400}H_{802}$ liquid simulated by Stephanou *et al.* (2010) as 39 Å, which they calculated according to Eq. (6) rewritten as $a_s = R^2/\langle L \rangle$. These values for a also compare favorably with the value of 36 Å determined experimentally for a polyethylene at 413 K [Fetters *et al.* (2007)], and the value of $N_e = 6.02$ compares reasonably well with the experimental value of 6.89 for the same liquid [Fetters *et al.* (2007)].

The expression used to calculate the number of entanglements, $Z = \langle L \rangle^2 / R^2$, is based on the assumption that the chain primitive paths obey Gaussian statistics and that entanglement strands between "kinks" in the primitive paths are interpreted as Kuhn steps. These assumptions break down under flow conditions as the chains deform and orient, and hence the measure of the number of entanglements used above becomes ill-defined. The Z1 code provides, besides $\langle L \rangle$, an additional quantity, $\langle Z_k \rangle$, based on the number of kinks along the three-dimensional primitive path of each chain, which in some unclear way is proportional to the number of entanglements. Assuming that the kinks represent junctures between entanglement strands, the average $\langle Z_k \rangle$ is calculated by the Z1 code, which is not restricted to Gaussian statistics and hence remains valid under flow conditions. Everaers (2012) offered an explanation for the empirical evidence [including that of Baig *et al.* (2010) and that presented below] which consistently suggests a proportionality factor of approximately two. Consequently, we will use this quantity in Sec. IV B describing the shear results rather than Z, and simply refer to it as the number of entanglements. Under quiescent conditions, $\langle Z_k \rangle = 9.91$, which is about twice the value of Z. It remains rather ambiguous, however, what exactly is the physical meaning of the concept of an "entanglement."

The ratio between τ_d and τ_R is expressed using Eqs. (4) and (5) as [Doi and Edwards (1986)]

$$\frac{\tau_d}{\tau_R} = 3Z. \tag{7}$$

The friction coefficient can be estimated using the diffusion coefficient of the chain center of mass, D_G. For times $t \gg \tau_d$, the diffusion coefficient is given by [Doi and Edwards (1986)]

$$D_G = \frac{k_B T a^2}{3N^2 \xi b^2}. \tag{8}$$

Using Eqs. (5) and (8), it is evident that

$$\tau_d = \frac{1}{3\pi^2}\frac{R^2}{D_G}. \tag{9}$$

Here, D_G is directly proportional to the slope of the center-of-mass mean-square displacement (MSD) versus time via [Doi and Edwards (1986)]

$$D_G = \lim_{t\to\infty} \frac{1}{6t}\left\langle \left(R_G(t+\tau) - R_G(\tau)\right)^2 \right\rangle. \tag{10}$$

It assumes the value of 1.0490×10^{-11} m^2/s based on the equilibrium simulation results for $t \gg \tau_d$; see Fig. 2. The disengagement timescale is thus calculated to be 273 ns using Eq. (9). The longest relaxation time obtained from the three-exponential fit (231 ns) is within 15% of this value. According to Eq. (7), the theoretical value of Rouse time is 18 ns.

Characteristic times of the system at equilibrium can also be determined by analyzing the segmental MSD versus time. This graph can also be used for calculation of other characteristic times of the system. The segmental MSD is defined as $\varphi(t) = \langle (r_n(t+\tau) - r_n(\tau))^2 \rangle$ [Doi and Edwards (1986)], where $\mathbf{r}_n$ is the position vector of the n-th monomer (i.e., the n-th -CH_2- unit). In order to minimize chain-end effects, only 50 monomers in the middle of the chains were included in these calculations. Figure 3 shows the segmental MSD as a function of time. Four different regimes (three characteristic breaks) can be observed in these plots. For a very short time, the segment does not feel the constraints of the network and it is known that $\varphi(t) = 2Nb^2(t/\pi^3\tau_R)^{1/2} \cong a^2$ [Doi and Edwards (1986)]. Therefore, the slope of a log-log plot is approximately 1/2 at very short times such that the average segmental displacement is much less than the tube diameter. According to Doi and Edwards (1986), the entanglement timescale, τ_e, is related to the segmental MSD as

$$\varphi(\tau_e) = 2Nb^2(\tau_e/\pi^3\tau_R)^{1/2} \cong a^2. \tag{11}$$

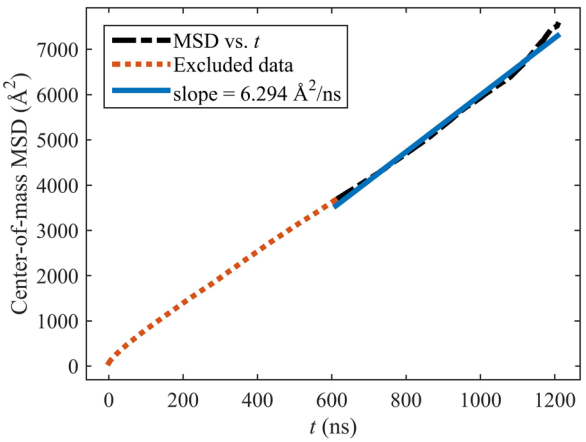

FIG. 2. MSD of the chain center of mass versus time. The solid line corresponds to the best linear fit to data for times much greater than the disengagement time.

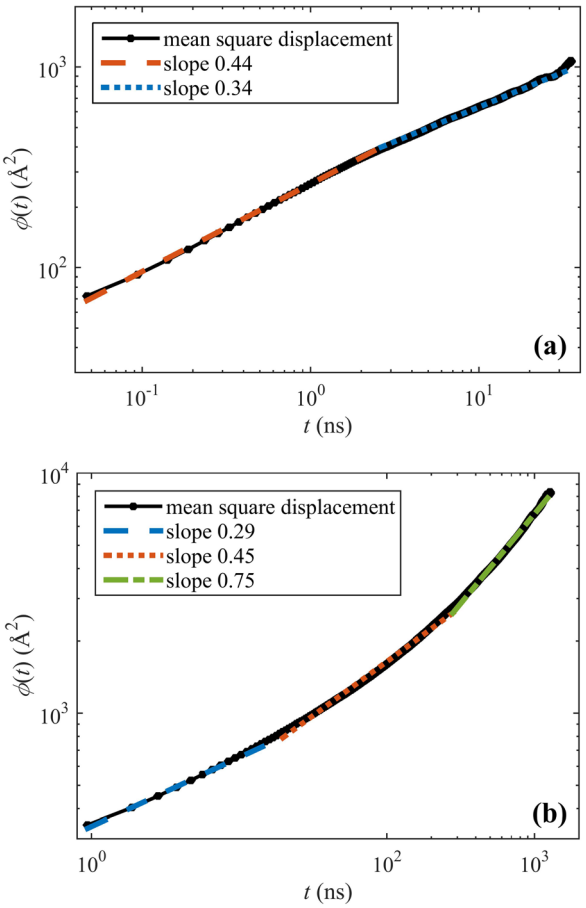

FIG. 3. Short (a) and long (b) timescale segmental MSD versus time of the centermost chain atomic units.

Substituting Eqs. (7) and (9) into (11) results in

$$\tau_e = \frac{\pi}{36}\frac{R^2}{D_G Z^3}. \tag{12}$$

Using Eqs. (7) and (9), Eq. (12) can be expressed relative to the other system timescales as

$$\frac{\tau_d}{\tau_e} = \frac{12}{\pi^3}Z^3 \quad \text{and} \quad \frac{\tau_R}{\tau_e} = \frac{4}{\pi^3}Z^2. \tag{13}$$

Accordingly, the theoretical value of τ_e is 5.1 ns. The very short time dynamics ($t < \tau_e$) are displayed in Fig. 3(a), where the initial slope is calculated to be 0.44 and then 0.34 for later times. The point where the slope changes is taken as corresponding to the entanglement time [Doi and Edwards (1986)]. Equation (11) indicates that the slope should assume the value of 0.5 at very short times, which is somewhat higher than the value indicated by the simulations.

For $t > \tau_e$, the motion of the segment perpendicular to the primitive path is restricted, but the motion along the primitive path is free. It is known that $\varphi(t) \cong a(k_B T\, b^2 t/\xi)^{1/4}$

for $\tau_e \leq t \leq \tau_R$ and $\varphi(t) \cong a(k_B T\, t/N\xi)^{1/2}$ for $\tau_R \leq t \leq \tau_d$ [Doi and Edwards (1986)]. Hence, the segmental MSD versus time curve has a slope of 1/4 in the region $\tau_e \leq t \leq \tau_R$ and a slope of 1/2 in the time region $\tau_R \leq t \leq \tau_d$. From Fig. 3(b), these slopes are 0.29 and 0.45, respectively, which approximate the expected values. For $t \geq \tau_d$ the dynamics are governed by the reptation process, where the segmental MSD is known to follow $\varphi(t) \cong \frac{k_B T\, a^2}{N^2 \xi b^2} t$, indicating a slope of unit value [Doi and Edwards (1986)]. The slope, however, turns out to be 0.75, which is sublinear; we assume that this discrepancy is due to the dynamical nature of the entanglement network.

The entanglement, Rouse, and disengagement times can be determined from the breaks in the curves of Fig. 3. These are estimated to be 2.6, 20, and 279 ns, respectively. The entanglement time matches very closely with the value of 2.9 ns estimated by Stephanou *et al*. (2010) for this liquid using the same method of determination. These authors did not report the Rouse time for this fluid, but they estimated the disengagement time as 489 ns, which is significantly more than the value of 279 ns obtained from the present simulations; however, our value compares well with that of 273 ns calculated from reptation theory. The Rouse time of 20 ns also compares well with the value of 18 ns calculated according to tube theory.

In order to compare the dynamics of the $C_{400}H_{802}$ melt with those of an analogous bead-rod chain in dilute solution, three parameters are needed to set the properties of the bead-rod chain. Two of these have already been determined: $N = 32$ and $b = 16.5$ Å. The final parameter, the friction coefficient, was set using the longest relaxation time of the dense liquid simulation, which was 231 ns. The autocorrelation function of the end-to-end vector can be expressed as [Doi and Edwards (1986)]

$$\langle \mathbf{R}(t+\tau) \cdot \mathbf{R}(\tau) \rangle = Nb^2 \sum_{p=1,3,\ldots} \frac{8}{p^2 \pi^2} \exp\left(-\frac{tp^2}{\tau_l} \right), \tag{14}$$

where p is the Rouse mode and τ_l is the longest system relaxation time, which typically takes on the meaning of the Rouse time, τ_R; however, once the system becomes reptative, the longest relaxation mode ($p = 1$) is associated with the disengagement time and the second longest relaxation mode ($p = 3$), can in some sense be viewed as a "Rouse time" for an entangled, reptative system. This viewpoint is supported by the comparison with reptation theory and the dense liquid data, as discussed above and presented in Fig. 3 and Table I. Note that the data for the three-exponential fit from Table I appear to confirm this; i.e., $231/28 = 8.25 \approx 9$, as would be expected from Eq. (14). Accordingly, the friction coefficient can be calculated for an assumed value of τ_l according to [Doi and Edwards, 1986]

$$\tau_l = \tau_R = \frac{\xi N^2 b^2}{3\pi^2 k_B T} \tag{15}$$

as 1.6×10^{-11} N s m^{-1}. Here, we must correlate the longest relaxation times of the two systems to obtain the correct equilibrium responses, even though this amounts to the Rouse time for the dilute solution and the disengagement time for the melt. With N, b, and ξ thus specified, a BD simulation of the bead-rod chain solution was carried out under quiescent conditions. The ensemble averages $\langle R^2 \rangle$ and $\langle R_g^2 \rangle$ were calculated as 8452 and 1442 Å^2, respectively; these correspond to the values of 8482 and 1369 Å^2 obtained in the melt simulation, as expected. A fit of the autocorrelation function $\langle \mathbf{u}(\tau) \cdot \mathbf{u}(\tau + t) \rangle$ with a sum of two exponential functions, as shown in Fig. 4, revealed

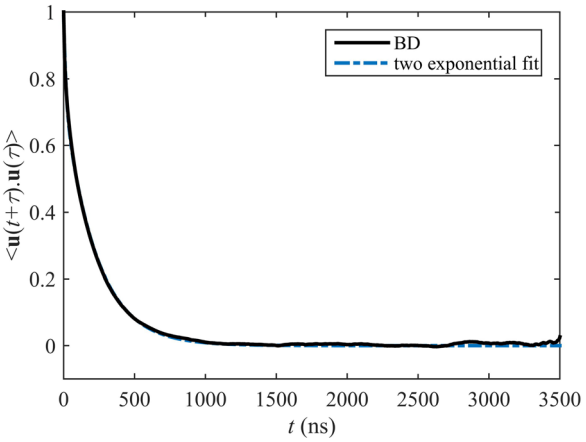

FIG. 4. Autocorrelation function of the unit end-to-end vector vs time of the BD simulation under quiescent conditions and a fit using a sum of two exponential functions.

timescales of 16 and 226 ns. The longer of these corresponds well to the value of 231 ns used to calculate ξ, demonstrating that the correct equilibrium dynamics have been incorporated into the mesoscopic bead-rod chain model. Note that the shorter timescale is the same as the Rouse time determined by the two-exponential fit of the NEMD data (see Table I), and lies in the rough neighborhood of 226 ns/9 = 25.1 ns, which is the timescale of the third relaxation mode predicted by Eq. (14) when $p = 3$.

In summary, the principal timescales deduced in this section were presented in Table I. As a whole, they appeared to be fairly consistent with each other over all methods of calculation. They also demonstrated that the $C_{400}H_{802}$ melt simulated in this study appears to be described fairly well by standard reptation theory at equilibrium, which is somewhat surprising given the low number of entanglements per chain (5.15) that it possesses; this places the liquid in the semientangled regime where reptation concepts are not as well defined as in the fully entangled state. This is a fortunate occurrence, however, in that it will allow us to discern clearly the important changes away from reptative behavior in Sec. IV B once sufficiently high shear rates have been attained.

B. Steady shear flow properties

The molecular dynamics and BD simulations described in Sec. IV A were extended to nonequilibrium conditions for $Wei \in [1.06,\ 22\ 250]$. The primary focus of the present article is on the rotational dynamics of the individual chain molecules composing the dense polyethylene liquid, which were not thoroughly examined by Baig *et al.* (2010). Nevertheless, the prior results served to test the consistency of our results (and theirs), as all of the bulk-average properties as functions of Wi reported by Baig *et al.* were reproduced quantitatively by the present suite of simulations; therefore, there is no need to repeat all of these data in the following text. We will focus only on those bulk-average properties whose characteristics are directly impacted by the individual chain rotation and retraction dynamics to make clear the effect that these unexpected chain motions have upon the macroscopic system properties.

The rotation and retraction cycles of individual chains comprising the $C_{400}H_{802}$ melt are displayed in Fig. 5(a) for a single chain chosen at random for $Wi = 10\ 600$. As evident from the plot, the chain is constantly experiencing both rotation and retraction of a quasi-periodic nature, similarly to previous studies of short-chain, unentangled polyethylene

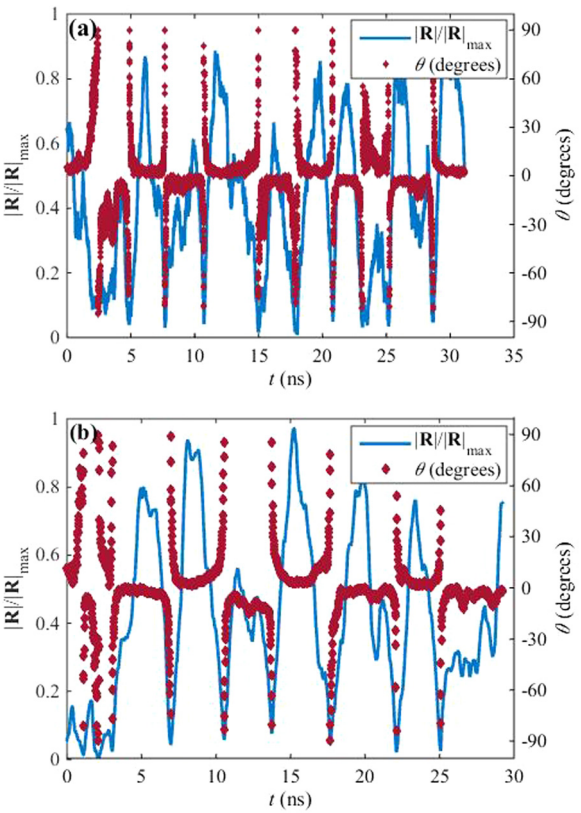

FIG. 5. Plots of the normalized end-to-end distance and orientation angle vs time for (a) a random chain in the dense liquid NEMD simulation and (b) a bead-rod chain from the free-draining dilute solution BD simulation. Both sets of data are for simulations at $Wi = 10\,600$.

$C_{78}H_{158}$ [Kim *et al.* (2009, 2010)]. During a typical period, the chain retracts from a highly extended configuration ($|\mathbf{R}|/|\mathbf{R}|_{max} \to 1$) to a tightly packed coil ($|\mathbf{R}|/|\mathbf{R}|_{max} \to 0$), which is even more compact than the equilibrium average random coil of $|\mathbf{R}|/|\mathbf{R}|_{max} = 0.18$. At the minimum point of the period, the orientation of the chain flips quickly as the chain ends pass each other at the instant of closest contact, after which the chain quickly expands once more to a highly stretched configuration. Although depicted for only a single random chain, the behavior of all molecules within the system is essentially the same, providing a much richer dynamics to the flow response of this melt than could have been imagined for this moderately entangled polymeric liquid. Indeed, this behavior is very similar to that observed by Edberg *et al.* (1987) for very short *n*-alkanes (butane and decane), where it would not be completely unexpected.

The periodic rotation and retraction cycles observed in the melt are very similar to those that occur within a dilute solution of a free-draining, bead-rod chain undergoing a high shear-rate flow. Figure 5(b) displays the dynamics derived from the BD simulations of the mesoscopic analog of the polyethylene liquid at the same value of *Wi* (10 600) as depicted in Fig. 5(a). Similar qualitative features can be noted, as well as essentially the same quantitative values of the rotational period and average molecular extension and compression. Hence the rotation/retraction dynamics of the polyethylene melt are provocatively similar to those of macromolecular dilute solution, which is quite surprising given the moderately entangled nature of the dense liquid. This provides initial evidence

that the entanglement network of the $C_{400}H_{802}$ liquid must be at least partially destroyed by the shear flow.

Snapshots from a typical period of a random chain of the NEMD simulations at $Wi = 10\,600$ are displayed in Fig. 6(a). A rotational period begins by either one or both chain ends diffusing backward along the backbone contour toward the center of the chain in a hairpinlike configuration, forming a tightly packed coil, which grows in size as the other chain end retracts toward the chain center. This compact molecular configuration then experiences an almost instantaneous flip in direction of the end-to-end vector, after which each chain end diffuses back along the molecular backbone until the chain is once again highly extended. This hairpinlike diffusion of the chain ends along the molecular backbone clearly requires an absence of interchain entanglements, and appears to possess the characteristics of anisotropic diffusion through cylindrical tubes formed by neighboring highly stretched chains, as hypothesized by Kim *et al*. (2009, 2010) and Kim *et al*. (2011).

Figure 6(b) shows similar configurations adopted by the bead-rod chain in dilute solution as simulated by BD at the same value of Wi as above. It is evident that the chain configurational rotation and retraction dynamics are very similar to those of the polyethylene dense liquid, with the only minor differences being that the bead-rod chain

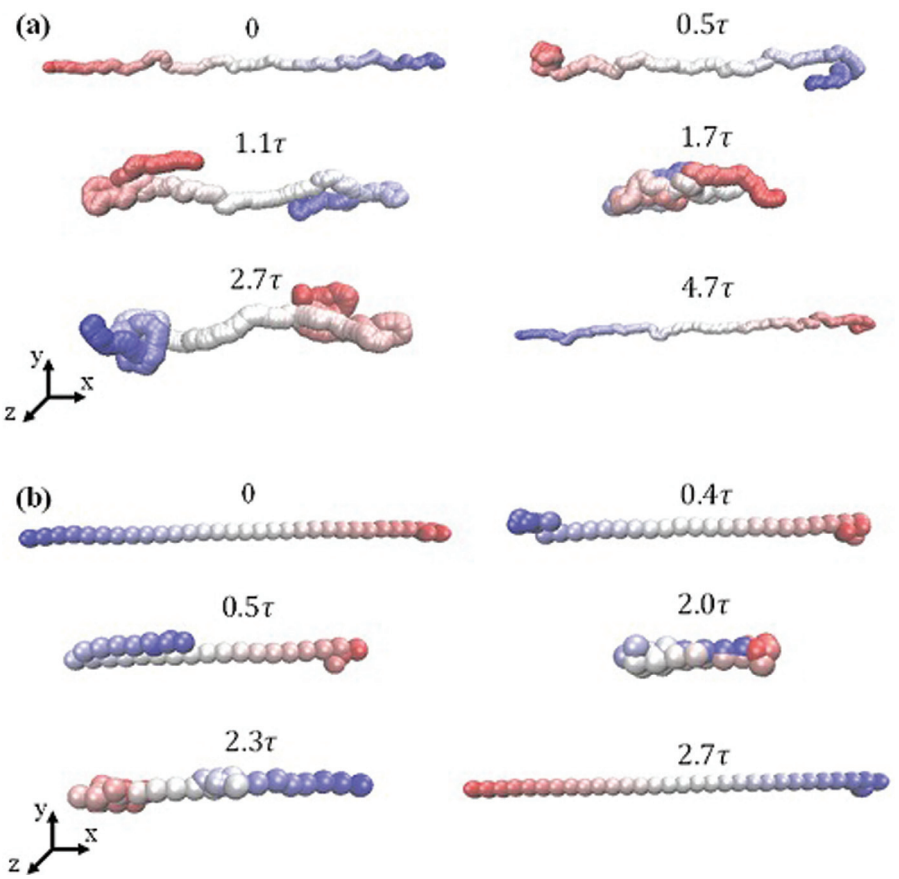

FIG. 6. Configuration snapshots of a randomly chosen single chain at various incremental time values from the (a) NEMD and (b) BD simulations at $Wi = 10\,600$. Setting the first configuration at a reference time of 0, snapshots correspond to time instants labeled as multiples of the longest system relaxation time ($\tau = 2.03$ ns for NEMD and 2.88 ns for BD).

configurations are more compact due to the lack of excluded volume interactions. These snapshots serve to reinforce the evidence of the lack of entanglements in the melt at high shear rates, since the observed configurations are very similar to those of the dilute solution. The remarkable similarity of dilute solution properties in a theta solvent and those of a melt under quiescent conditions has been a hallmark of polymer theory for over seventy years; it appears there is also a great deal of similarity under a strongly shearing flow as well. At high shear rates, the polyethylene chains behave similarly to analogous molecules in dilute solution, experiencing a mean-field force that acts through isotropic drag on statistical Kuhn segments of the atomistic chain.

The configurational behavior observed above at $Wi = 10\,600$ is rather straightforward to interpret due to the similarities with dilute solution behavior, as described above, and also due to the very high applied shear rate which places the system response well within the Wi range where the chain dynamics are dominated by the rotation and retraction cycles and all entanglements have essentially been destroyed—see below. At intermediate Wi, the configurational dynamics are more difficult to interpret since chain stretching is still playing a competing role in dictating the systems response and the entanglement network has yet to be completely annihilated.

Figure 7 shows plots of the rotation/retraction cycles of the chains within the melt and solution at $Wi = 106$. Several features are obvious in contrast with Fig. 5 at $Wi = 10\,600$.

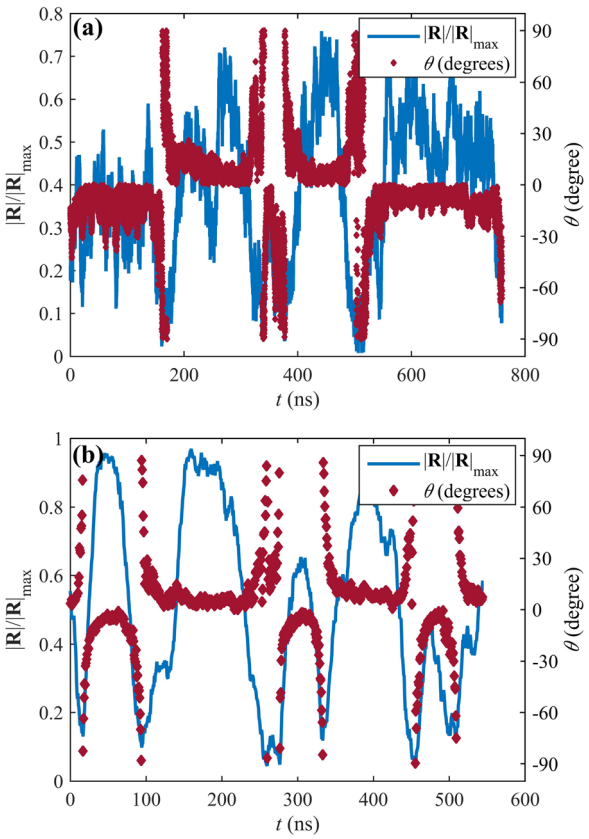

FIG. 7. Plots of the normalized end-to-end distance and orientation angle vs time for (a) a random chain in the dense liquid NEMD simulation and (b) a bead-rod chain from the free-draining dilute solution BD simulation. Both sets of data are for simulations at $Wi = 106$.

First, the degree of chain stretching at the apex of the rotational cycle is much lower at $Wi = 106$, as expected. Nevertheless, the rotational motion at $Wi = 106$ is as readily apparent as it was at the higher value of Wi. Also, the rotational cycles are far less regularly periodic than at $Wi = 10\,600$. Furthermore, the timescale of the rotation is two orders of magnitude higher than at the higher value of Wi, and the molecules remain in their stretched state for much longer portions of the overall periodic cycle.

Figure 8(a) presents configurational snapshots of random chain at a number of time increments at $Wi = 106$ for both the dense liquid and dilute solution simulations. There are some subtle yet crucial differences between the configurational dynamics at this value of Wi compared to the much higher value of Fig. 6. Most apparent is the fact that neither the atomistic chain nor the bead-rod chain experiences nearly as great of a degree of extension at the apex of its rotational cycle. However, another subtle difference is that the atomistic chain does not fully collapse at the moment of the orientation angle flip, as at the higher Wi number, whereas the bead-rod chain experiences essentially the same configurational collapse to a very compressed structure at the middle of its cycle. Furthermore, the motion of the atomistic chain no longer resembles that of a collapsing and extending structure, but appears to move linearly along the chain backbone like a

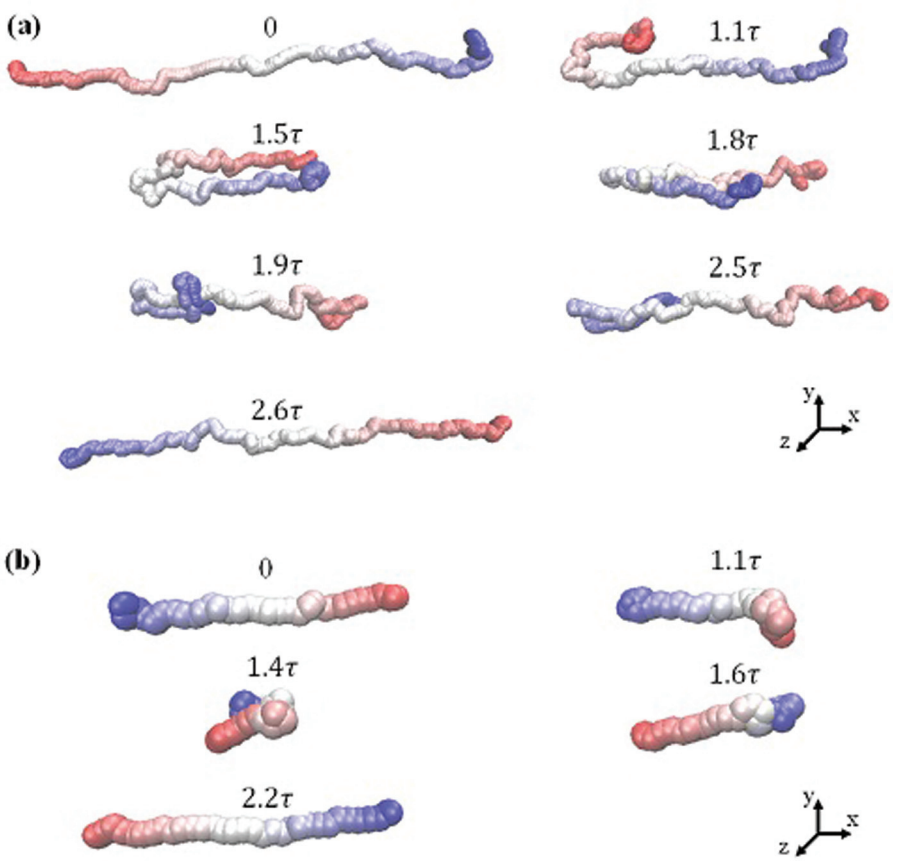

FIG. 8. Configuration snapshots of a randomly selected single chain at various incremental time values from the (a) NEMD and (b) BD simulations at $Wi = 106$. Setting the first configuration at a reference time of 0, snapshots correspond to time instants labeled as multiples of the longest system relaxation time ($\tau = 48.8$ ns for NEMD and 61.9 ns for BD).

rope passing over a pulley, or as if diffusing around some internal obstacles. One hypothesis is that at this lower value of Wi there still exist a significant number of entanglements such that the atomistic chains are forced to diffuse around the obstructions of neighboring chains. In the BD simulations of the dilute solution, however, there are by default no entanglements to impede the segmental motion, and hence the bead-rod chain experiences the same diffusive motion regardless of the value of Wi.

The dynamics of the dense liquid and dilute solution can be quantified by determining the characteristic times of the system responses, which now include a rotational timescale that characterizes the period of the tumbling/retraction cycles of the chains. The first timescale is associated with the longest timescale of the liquid at equilibrium, which we formerly referred to as the disengagement time. As Wi is ramped up, it is clear that the idea of a reptation or disengagement timescale becomes ambiguous as the entanglement network within the fluid relaxes and ultimately vanishes completely. Consequently, for the remainder of this article we will refer to this timescale simply as the longest relaxation time, even though later on the rotational timescale will actually be larger than this quantity. These relaxation timescales can be determined using autocorrelation functions of various components of the unit end-to-end vector and fitted to known functions, as we discussed above for the quiescent fluids. At low values of Wi, we used a two-exponential summation to determine the longest and Rouse timescales, whereas for Wi in the strongly nonlinear viscoelastic regime, we used the single exponential function with an embedded cosine dependence [analogous to Eq. (1)] to fit the longest and rotational timescales.

At $Wi = 1$ and 10, the autocorrelation functions, $\langle \mathbf{u}_i(\tau) \cdot \mathbf{u}_i(\tau + t) \rangle$, of the dense liquid and the dilute solution decay monotonically in a qualitatively similar fashion to those of the quiescent fluids, as shown in Figs. 1 and 4. For $Wi \geq 50$, however, the autocorrelation functions of both liquids display an initial monotonic decrease with time, but then pass below the zero axis and then experience a damped oscillation that eventually decays to zero over about two time periods of the cycle. This behavior is shown in Fig. 9 for both liquids, as well as the fits to this data using Eq. (1), at $Wi = 106$ and 10 600.

The longest relaxation times of the dense liquid and dilute solution are displayed in Fig. 10 as functions of Wi. At $Wi = 1$ and 10, this timescale does not change appreciably from the two-exponential fit of either liquid under quiescent conditions (225 and 235 ns, respectively—see Table I). This is the behavior expected from classical reptation theory of the disengagement time, which appears to remain valid well into the nonlinear viscoelastic regime, at least up to $Wi = 10$. In the linear viscoelastic regime (up to $Wi = 1$), the second timescale of the melt and solution remain approximately constant at 19 and 14 ns (based on a two-exponential fit), respectively, compared to the equilibrium values of 16 and 18 ns. As the shear rate is increased into the nonlinear regime, the Rouse time of the melt has decreased to 6 ns at $Wi = 10$, whereas that of the solution has essentially disappeared from the system response leaving only a single exponential decay.

For $Wi > 10$, both sets of data show a precipitous drop which becomes even more pronounced for $Wi > 1000$ where power-law fits provide slopes of -0.73 for the melt and -0.66 for the solution. Somewhere within $Wi \in [10, 50]$, the concept of a disengagement time begins to lose relevance; the longest timescale takes on more of a meaning in the sense of a characteristic time for decorrelation of the molecules' configurational states due to the rotation and retraction cycles of the chains. In other words, it defines a timescale over which the chain configurations decorrelate within the tumbling periods that they experience. The NEMD and BD data essentially display the same qualitative trends, but there is a quantitative difference between the two data sets as the melt relaxation times are slightly but consistently shorter than those of the solution. The same trend was noticed by Kim *et al*. (2010), who argued that the bead-rod chain configurations in dilute

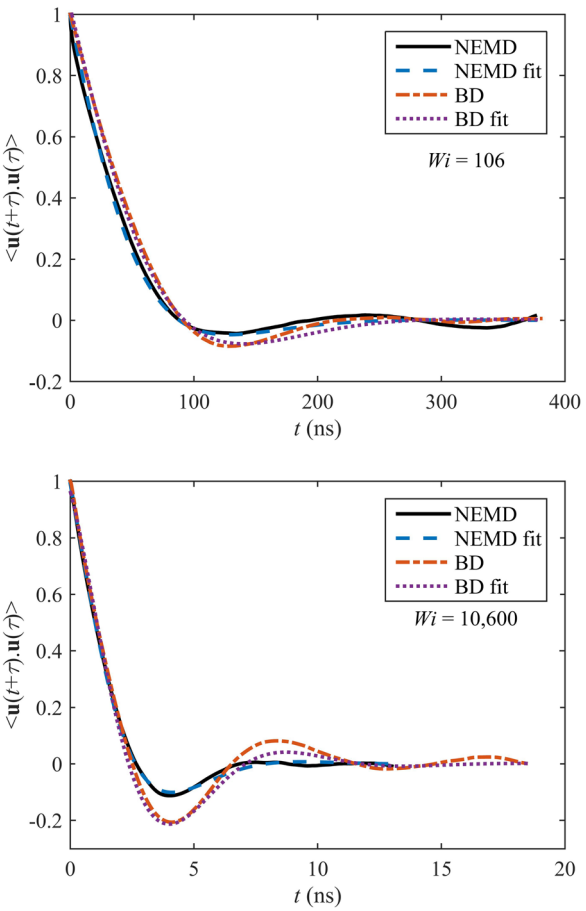

FIG. 9. Plots of the autocorrelation function of the unit end-to-end vector vs time at $Wi = 106$ and 10 600 for the atomistic (NEMD) and bead-rod (BD) chain liquids and fits to the data using Eq. (1).

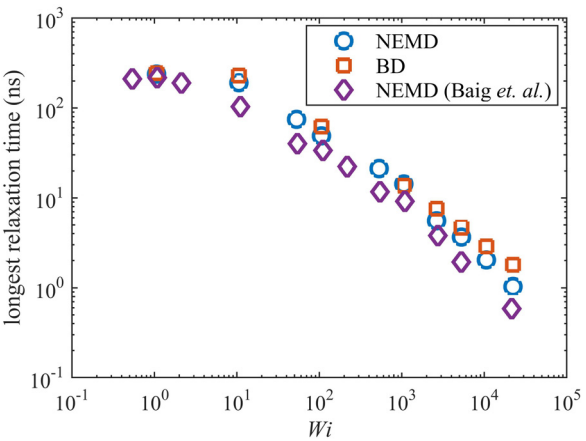

FIG. 10. The longest system relaxation time for the atomistic (NEMD) and bead-rod (BD) chain liquids as functions of Wi. For $Wi > 1000$, the slopes of power-law fits are -0.73 and -0.66, respectively. Also shown are data of Baig *et al*. (2010).

solution would decorrelate over a longer timescale since the tumbling cycles would be more regular because the bead-rod chains do not experience topological constraints due to either entanglements or excluded-volume interactions, as occur within the dense liquid.

Figure 10 also displays the data for the longest relaxation time of Baig *et al*. (2010) for the $C_{400}H_{802}$ melt. The results are qualitatively similar between their melt system and ours; however, their relaxation times are consistently a factor of 1.7 less. If we had used simply a stretched exponential of the form of Eq. (3) to fit our data, our relaxation times would have been quantitatively very close to those of Baig *et al*. Therefore, it is our interpretation that the lower values of these authors are due to the neglect of the rotational timescale, as appearing in Eq. (1). It is apparent that there is some degree of coupling between these two relaxation times (i.e., longest and rotational), and that these two quantities describe different facets of the same configurational dynamics. We will discuss this issue more thoroughly below.

The rotational timescale derived from Eq. (1) has been plotted versus Wi in Fig. 11. This timescale is essentially undefined for $Wi < 50$, and then becomes clearly discernible in the autocorrelation curves, such as those in Fig. 9, for all greater values of Wi for the melt and for $Wi \geq 100$ for the solution. These timescales are rather high at low Wi, with values of several hundred nanoseconds, which are greater even than the equilibrium disengagement time of 231 ns. Both the melt and the solution again exhibit power-law behavior, but in this case the slopes are nearly identical; i.e., -0.78 and -0.80 for the melt and solution, respectively. The rotational timescale of the melt is slightly higher than that of the solution at intermediate Wi, although the results are within statistical error of each other at low and high Wi. Similar behavior was observed by Kim *et al*. (2010) for a $C_{78}H_{158}$ liquid. A higher rotational timescale implies that the rotation and retraction period is longer, and hence it is to be expected that the entangled melt would exhibit larger timescales than the unentangled solution. In the regime where the melt is experiencing a high rate of entanglement destruction, therefore, its characteristic time is higher than that of the solution because there remain a small but significant number of constraining entanglements. However, once the entanglement network has been completely destroyed, one might expect the two timescales to be quantitatively the same. We will discuss this issue in more detail later on.

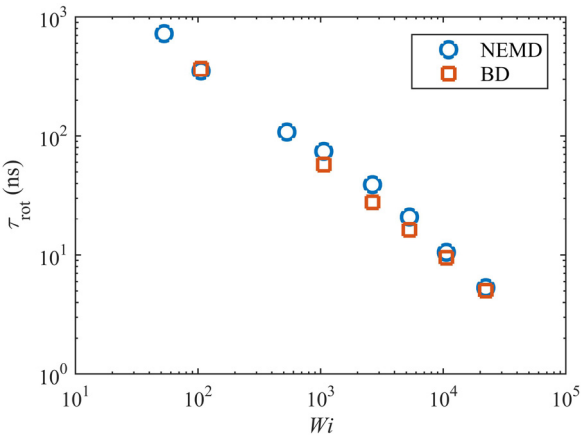

FIG. 11. The rotational timescales for the atomistic (NEMD) and bead-rod (BD) chain liquids as functions of Wi. For $Wi > 1000$, the slopes of power-law fits are -0.78 and -0.80, respectively.

It is natural to wonder how the dynamics of the rotational cycles are affected by the vorticity of the macroscopic flow field. This is a difficult question to address, however. Figure 12 displays plots of the rotational frequency, defined as the reciprocal of the rotational timescale described above. Also shown in this figure is the rotation rate of the macroscopic velocity field, as quantified by half of the applied shear rate. Both the melt and the solution exhibit rotational frequencies that are two orders of magnitude slower than the rate of macroscopic rotation at all values of *Wi*. The slopes of the melt and solution curves are 0.88 and 0.80, respectively, as compared to a unit slope of the macroscopic rotation rate. Although it is most likely the macroscopic rotation of the fluid that induces the diffusion of the chain ends, thus beginning their rotation/retraction cycles, it is evident that the diffusive motion of the chain segments is not directly influenced by the rotational timescale of the shear flow, although there is some correlation between the two processes. Whatever the connection may be, there is strong evidence that the melt and dilute solution experience the same mechanism, given the high degree of quantitative similarity exhibited by their rotational timescales.

Figure 13 quantifies the differences between the longest and characteristic rotational periods by examining their ratios of melt timescales over solution timescales. The point to emphasize here is that both ratios are very close to unity, irrespective of the value of *Wi*. There are some minor, discernible trends in the data, which were discussed above, but for the most part, this plot displays clearly the similarity between the dynamics of the atomistic macromolecule and the bead-rod chain.

The ratio of the rotational period to the longest timescale is displayed in Fig. 14 for both the melt and dilute solution. The ratio for the melt is higher than that of the solution, but not significantly so in light of the multiplication of statistical uncertainty associated with forming the ratios. The melt data are fairly scattered, but not over a wide range of values; its trend, however, is clear in that this ratio decreases with increasing *Wi*. In the zero-shear limit, the rotational timescale goes to infinity, whereas the longest relaxation time assumes its equilibrium value of 231 ns. The data for the dilute solution are qualitatively similar, although much more precise than that of the melt, presumably because of the clearer, more periodic nature of the tumbling cycles when compared to the melt. The decreasing trend indicates that the longest relaxation time decreases at a slower rate than the rotational period, which could be due to the fact that the configurational correlation quantified by the longest relaxation time persists to a greater extent for chains undergoing

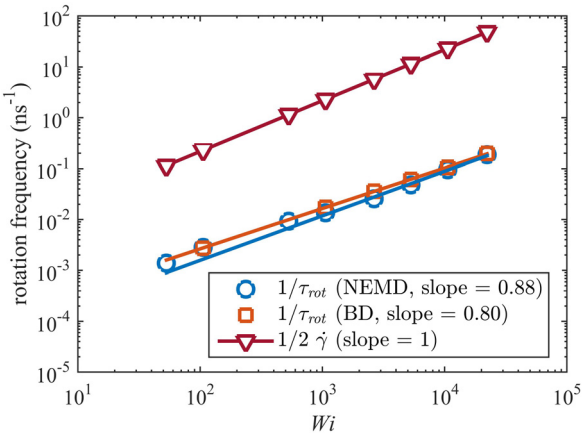

FIG. 12. Rotational timescales of the melt (NEMD) and dilute solution (BD) versus *Wi* compared to the macroscopic fluid rotation rate, as quantified by half the vorticity.

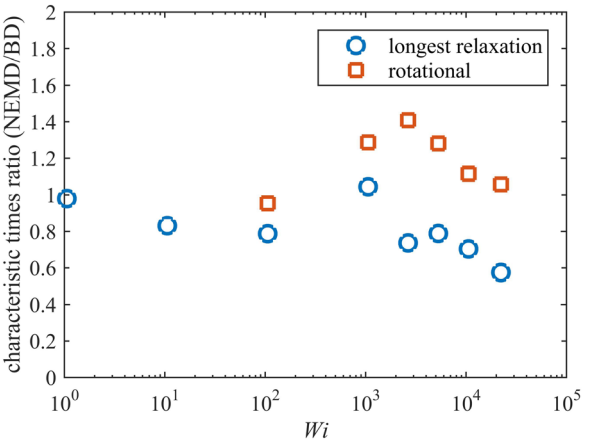

FIG. 13. The longest relaxation and rotational timescales are compared by taking ratios of those of the melt with respect to those of the dilute solution.

the higher frequency rotational cycles at larger values of *Wi*, where the rotational cycles displayed by the autocorrelation function of the unit end-to-end vector are much more clearly defined.

Given the periodic rotational dynamics of the individual molecules comprising the polyethylene melt, it is natural to wonder how this unexpected behavior affects the bulk-average properties of the liquid. In general, there are several physical effects that take place under imposition of conditions of high shear that occur simultaneously once a critical value of *Wi* has been achieved. These are chain deformation, chain orientation, and chain rotation/retraction. At low shear rates, only the chain orientation changes dramatically, but once well within the nonlinear viscoelastic regime, the orientation of the polymer chains remains relatively constant whereas the chain deformation and then rotation play increasingly important roles in determining the bulk-average properties of the liquid.

First, we examine the topological characteristics of the dense $C_{400}H_{802}$ melt to provide insight later into how rotational chain dynamics affect bulk-average fluid properties.

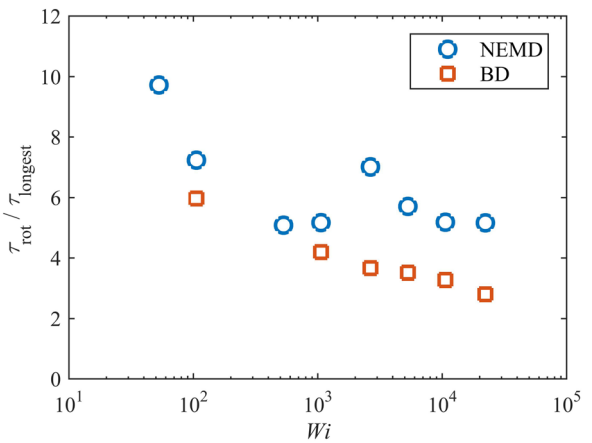

FIG. 14. Ratios of the rotational periods with respect to the longest relaxation times for the melt (NEMD) and dilute solution (BD).

Figure 15 displays topological data for the dense liquid as obtained by applying the Z1 code to the data of the NEMD simulations. Figure 15(a) presents data for $\langle Z_k \rangle$, which we will refer to as the "number of entanglements per chain," as a function of Wi. At low Wi, the number of entanglements decreases very slowly as the chains deform mildly from the random coil configurations they occupy at equilibrium. At $Wi = 1$, $\langle Z_k \rangle = 9.5$, which is very close to the quiescent value of 9.91. As the shear rate enters the nonlinear

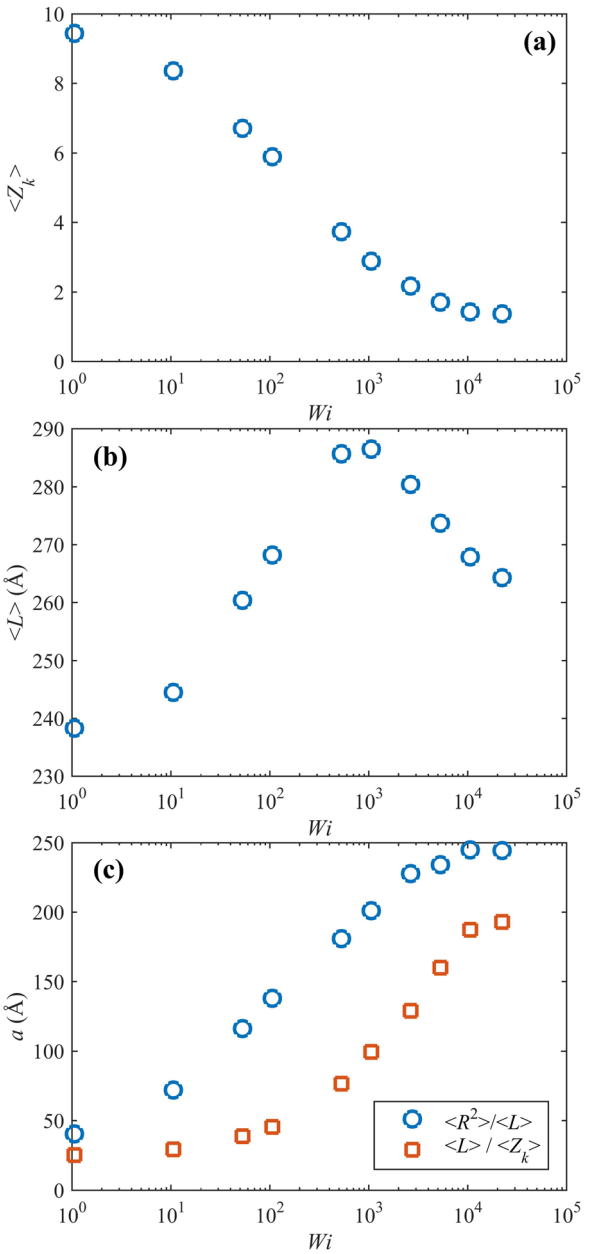

FIG. 15. Plots of topological features (a) average number of entanglements per chain, (b) average primitive path length, and (c) effective tube diameter versus Wi for the dense liquid NEMD simulations calculated via two different formulae.

viscoelastic regime, the decrease in $\langle Z_k \rangle$ becomes more significant due to the high degree of strain stretching and aligning (see below) that occurs in this shear flow region. In essence, as the chains stretch and orient in response to the flow field, entanglements are destroyed in proportion to the elongational state of a given chain. Apparently, the uncoiling process eliminates many of the entanglements, allowing the chains to glide by each other more freely, ultimately resulting in a shear-thinning viscosity. This decrease becomes very dramatic once inside the range where chain rotation and retraction begins to occur at $Wi \approx 50$. It thus appears that there is a critical value of $\langle Z_k \rangle$ at which point the system dynamics change from flow-aligning to rotational, which appears to be approximately 5 and occurs at $Wi \approx 50$. This value of Wi is consistent with that obtained from the timescale analysis presented above. At very high shear rates, $\langle Z_k \rangle$ levels out at about 1.3 entanglements per chain, implying that the entanglement network within the flowing liquid has essentially been completely destroyed. Furthermore, the distribution of $\langle Z_k \rangle$ values is extremely narrow around this value, indicating that practically all chains are effectively completely disentangled. The same qualitative behavior for $\langle Z_k \rangle$ was first observed in shear flow by Kim *et al*. (2008b) for $C_{78}H_{158}$ and later by Baig *et al*. (2010) for $C_{400}H_{802}$.

Figure 15(b) is a plot of the average primitive path length versus Wi for the dense liquid. For $Wi < 1$, $\langle L \rangle$ increases slowly from its quiescent value of 209 Å as the chains slowly begin to stretch out in response to the imposed shear field. The magnitude of this response increases dramatically once Wi has entered into the nonlinear viscoelastic regime of severe chain stretching, and then even more dramatically once Wi crosses over into the rotational dynamics regime at $Wi \approx 50$. This steep increase continues up to $Wi \approx 1000$ as chain stretching and chain rotation begin to compete with each other to control the overall average value of $\langle L \rangle$: The chain elongation acts to increase $\langle L \rangle$, whereas the chain rotation tends to shrink it as the chains recoil and compress due to the elimination of entanglements. Up to $Wi \approx 1000$, the dramatic increase in the chain elongation more than offsets the slowly rotating dynamics of the individual chains; however, for Wi greater than 1000, the chain rotation occurs with sufficient frequency to enable it to compete effectively with chain stretching for dominance of $\langle L \rangle$. At very high Wi, the chain rotation and retraction cycles are so fast and frequent that the rotational dynamics dominate $\langle L \rangle$, causing it to decrease substantially with Wi at high shear rates. As in the case of $\langle Z_k \rangle$, the same qualitative behavior for $\langle L \rangle$ was first observed in shear flow by Kim *et al*. (2008b) for $C_{78}H_{158}$ and later by Baig *et al*. (2010) for $C_{400}H_{802}$.

The tube diameter is fairly constant within the linear viscoelastic regime, as depicted in Fig. 15(c): It increases only slightly from its quiescent value of about 40 Å. Once into the nonlinear viscoelastic regime, and ultimately into the rotational dynamics regime, it increases dramatically as the number of entanglements is reduced due to chain stretching and aligning. After the entanglement network has been completely destroyed at very high Wi, the tube diameter plateaus at a value of about 240 Å since it cannot grow further because $\langle Z_k \rangle$ has attained its minimal value. [Using the definition of a based on Eq. (6), with $Z = \langle L \rangle^2 / R^2$.] At these high shear rates, the chains are rotating more or less independently of the chains surrounding them. A similar behavior for a was observed in shear flow by Kim *et al*. (2008b) for $C_{78}H_{158}$ and by Baig *et al*. (2010) for $C_{400}H_{802}$. The diameter of the tube formed by surrounding stretched chains may somehow control the size of the compressed coil required to initiate a flip in the end-to-end vector orientation, but this is difficult to determine from the simulations; unfortunately, the average radius of gyration is dominated by the stretched chains, making a quantitative analysis of chain compression during the rotation and retraction cycle problematic.

The data for the tube diameter discussed above are based on Eq. (6) with $Z = \langle L \rangle^2 / R^2$, which is strictly valid only for Gaussian statistics near equilibrium; i.e., $a = \langle R \rangle^2 / \langle L \rangle$. Therefore, as Wi becomes significant, this expression probably becomes inaccurate. In Fig. 15(c), we also present data for the tube diameter based on the formula $a = \langle L \rangle / \langle Z_k \rangle$, which is based solely on topological features of the chain liquid that should remain valid at high Wi. As expected, the two quantities asymptote to the same value of about 40 Å at equilibrium, but the latter definition of the tube diameter plateaus at a lower value of roughly 200 Å. This is probably a better indicator of the variation of the tube diameter with shear rate, although the concept of a reptation tube probably breaks down once the entanglement number has been reduced to a sufficiently low value and the exact value of this quantity becomes meaningless.

The ensemble average orientation angle of the end-to-end vector with respect to the flow direction (in the flow-gradient plane) is displayed in Fig. 16 as a function of Wi. In the case of the dense liquid, the orientation angle drops precipitously from its zero-shear limiting value of 45° in the linear viscoelastic regime, and then decays toward 0° as Wi passes into the nonlinear viscoelastic regime where dramatic molecular stretching occurs. It continues its rapid decrease once within the Wi range where chain rotation and retraction begin to manifest in the system response to the shear field ($50 < Wi < 500$), and then saturates at a small, positive value of approximately zero as Wi grows larger than 1000 into the regime where chain rotation dominates the liquid's dynamical response. As evident from Fig. 5(a), the rotating chain end-to-end vectors are almost always pointed very close to the flow direction, even during the chain retraction phase, except for very brief intervals in which the vector flips orientation by approximately 180°. Consequently, at any instant most molecules are oriented in the same direction, and hence it would be very difficult to find evidence of molecular rotation from measures of the average orientation angle alone; i.e., the observed data actually track very well that which would be expected from any typical rheological model exhibiting a flow-aligning microstructure. Nevertheless, since the molecules remain aligned in the flow direction for most of their rotational cycles, an opportunity is provided for tube formation as well as entanglement slippage, provided the average molecular extension is high enough.

Also shown in Fig. 16 is the orientation angle of the chains in dilute solution, θ, which is based on the definition of the ensemble average of the unit end-to-end vector dyadic product, $\langle \mathbf{u}_i \mathbf{u}_i \rangle$ and calculated according to the Eigenvector associated with its principal

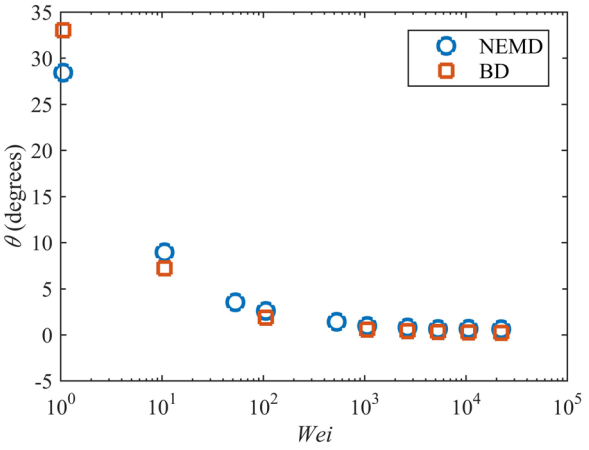

FIG. 16. Orientation angle vs Wi for the dense liquid (NEMD) and dilute solution (BD).

direction. This angle also drops rapidly from the zero-shear limit of 45° as *Wi* increases, approaching a high shear limit of 0°. Although qualitatively similar, the decrease in this case is more rapid at intermediate shear rates than in the case of the melt since the dilute solution is devoid of entanglements, allowing the chains to orient toward the flow direction at lower *Wi* than the dense liquid. However, once the entanglement network within the melt has been almost completely destroyed, both the dilute solution and the dense liquid display the same high shear limiting value of the orientation angle.

The mean-square of the end-to-end vector, $\langle R^2 \rangle$, of the dense liquid as a function of *Wi* is displayed in Fig. 17. At low values of *Wi*, it increases very slowly from its quiescent value of 8482 Å^2 within the linear regime, and then more rapidly once within the nonlinear viscoelastic regime of $Wi > 1$. As the chains elongate, the number of entanglements diminishes as well, allowing even further elongation with increasing *Wi*. Once within the regime where rotational effects begin to compete with chain extension, the dramatic rise in $\langle R^2 \rangle$ begins to abate, ultimately plateauing off and then starting to decrease at very high *Wi*. [This high shear-rate decrease is more obvious in the NEMD simulations of $C_{78}H_{158}$ of Kim *et al.* (2009).] The maximum extension of the chains under shear, roughly 65 000 Å^2, occurs at about $Wi = 10\,000$ and is well below the value of the fully extended chain of 265 225 Å^2, and is thus only 25% of the value of the completely stretched molecule. The reason for this is now apparent: Once the number of entanglements has been reduced substantially, there is no barrier to rotational motion and the chains spend much of their retraction cycles in configurations with much lower end-to-end vector magnitudes, which reduces the average value of $\langle R^2 \rangle$ substantially even though the chains do occupy nearly fully extended configurations for a brief part of the rotational periods.

Also displayed in Fig. 17 is the mean-square of end-to-end vector of the bead-rod chain versus *Wi* as calculated from the BD simulations. As in the case of the dense liquid, the bead-rod chain extends very slowly within the linear viscoelastic regime, tracking very closely the value of $\langle R^2 \rangle$ of the dense liquid. Once within the nonlinear viscoelastic regime, however, it increases much more rapidly than $\langle R^2 \rangle$ of the dense liquid, which is due to the fact that the chain in dilute solution is completely free of entanglements and is easily stretched, whereas the melt still contains a significant number of entanglements

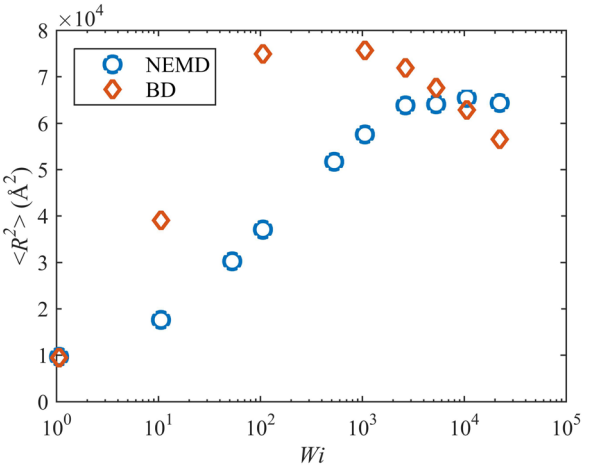

FIG. 17. Mean-square of the end-to-end vector versus *Wi* for the dense liquid (NEMD) and dilute solution (BD).

per chain at these values of Wi. The $\langle R^2 \rangle$ of the dilute solution eventually attains a maximum at about 80 000 Å^2 as the rotational dynamics begin to counterbalance the configurational stretching effect, and then for higher Wi $\langle R^2 \rangle$ continuously decreases. As the number of entanglements in the dense liquid decreases to a negligible value, the $\langle R^2 \rangle$ values of the bead-rod chain and the atomistic liquid once again become comparable.

The probability distribution function of the magnitude of the end-to-end vector is displayed in Fig. 18(a) for a number of Wi. The exhibited behavior is very intriguing, having first been identified for dense polyethylene melts in the case of $C_{78}H_{158}$ by Kim *et al.* (2009). At equilibrium and within the linear viscoelastic regime, the distribution is approximately Gaussian, as one would expect for a typical flow-aligning polymeric liquid model. However, once within the nonlinear regime, the distribution begins to widen toward the longer chains, and eventually a second peaks forms which quantifies the probability of finding highly stretched macromolecules. At the same time, the first peak shifts backward toward values even smaller than the quiescent value, indicating that more compressed chain coils than are present at equilibrium. Furthermore, the distribution is very spread out at high shear rates, overall, indicative of a system of chains with a wide

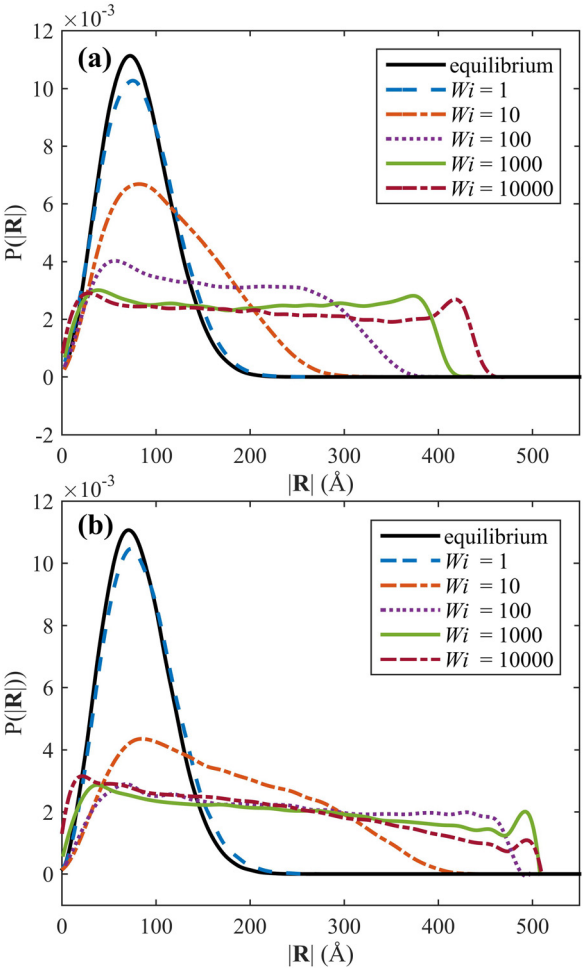

FIG. 18. Probability distribution of the magnitude of the end-to-end vector versus $|\mathbf{R}|$ for (a) the dense liquid and (b) the dilute solution at various values of Wi.

distribution of configurations. It has been recognized before [Kim *et al*. (2009, 2010); Baig *et al*. (2010)] that the first peak of the distribution is associated with the rotational and compressional states of the rotating chains at the reorientation point (i.e., where the end-to-end vector angle flips), whereas the second peak is determined by the highly stretched configurations of the chains at the apex of their cycles. The rather wide spread of the distribution at high *Wi* renders average measures of extension and orientation, such as $\langle R^2 \rangle$ of Fig. 17, practically meaningless.

Figure 18(b) shows the probability distributions for the dilute solution at the same values of *Wi* as presented in Fig. 18(a). The observed behavior is remarkably similar at all values of *Wi*, with the possible exception of $Wi = 100$, where the distribution is significantly more spread out for the bead-rod chain system than for the melt. We believe that this is a result of the fact that the bead-rod chain is completely free of entanglements, whereas the chains in the dense liquid are still constrained by roughly six entanglements per chain (according to the Z1 code), which significantly restrict their ability to elongate more substantially.

V. CONCLUSIONS

At first glance, the rotational dynamics observed in the dense liquid simulations were quite unexpected given the number of perceived entanglements per chain in the equilibrium system, which was approximately five. It is hard to imagine how a network of chains with so many entanglements could exhibit the type of rotational motion described above until one examines how the number of entanglements varies with increasing *Wi*. As evident from Fig. 15(a), the number of entanglements decreases dramatically with *Wi*, ultimately approaching a negligible value for very high *Wi*. The mechanism is now clear: As the shear rate increases, the chains stretch and align in the flow direction, which eliminates the majority of entanglements and provides effective tubes for molecular recoil and rotation, similarly to the short-chain macromolecules of $C_{78}H_{158}$ examined by Kim *et al*. (2009, 2010). Furthermore, it is worth pointing out that the onset of this behavior occurs at a fairly low *Wi* value, somewhere between 10 and 50 for the $C_{400}H_{802}$ melt, well within the range of process operations. As the flow strength increases, these individual chain rotation/retraction cycles increase in frequency as the number of entanglements declines. At equilibrium and low values of *Wi* within the linear and weakly nonlinear viscoelastic regime, reptation theory appears to work well for describing the dynamical features of the rheological behavior of the melt, which is generally the flow-aligning behavior one would expect from most rheological theories. However, as *Wi* obtains a value between 10 and 50, the constituent molecules begin to experience rotation and retraction cycles that compete with the average, flow-aligned configurational state, and the net effect of this balance between the two physical mechanisms is a region where the motion of a given molecule resembles fairly well those of a single chain experiencing anisotropic diffusion within a tube formed by its neighboring chains; such an idea was developed into a mesoscale model by Kim *et al*. (2011), as described in Sec. II. At very high *Wi* (>1000), the motion of the chains becomes essentially that of a single chain in dilute solution experiencing isotropic drag from the surrounding solvent molecules. Hence the analogy between dilute solutions of macromolecules in a theta solvent and dense polymer melts at equilibrium again becomes relevant at high strain rates. Overall, for the $C_{400}H_{802}$ liquid under investigation, we conclude that there are essentially three regions of flow behavior: a reptative region for $Wi \in [0, 10]$, a region of anisotropic segmental diffusion for $Wi \in [50, 1000]$, and a third region of behavior resembling that of a dilute solution at higher *Wi*.

ACKNOWLEDGMENTS

National Science Foundation provided computational resources under Grant No. CBET-0742679 to the PolyHub Virtual Engineering Organization as well as through the National Institute for Computational Science (NICS) by allocation of advanced computational resources (KRAKEN and DARTER).

References

Aust, C., M. Kröger, and S. Hess, "Structure and dynamics of dilute polymer solutions under shear flow via nonequilibrium molecular dynamics," Macromolecules **32**, 5660–5672 (1999).

Aust, C., S. Hess, and M. Kröger, "Rotation and deformation of a finitely extendable flexible polymer molecule in a steady shear flow," Macromolecules **35**, 8621–8630 (2002).

Baig, C., and V. G. Mavrantzas, "Multiscale simulation of polymer melt viscoelasticity: Expanded-ensemble Monte Carlo coupled with atomistic nonequilibrium molecular dynamics," Phys. Rev. B **79**, 144302 (2009).

Baig, C., B. J. Edwards, and D. J. Keffer, "A molecular dynamics study of the stress-optical behavior of a linear short-chain polyethylene melt under shear," Rheol. Acta **46**, 1171–1186 (2007).

Baig, C., B. J. Edwards, D. J. Keffer, and H. D. Cochran, "A proper approach for nonequilibrium molecular dynamics simulations of planar elongational flow," J. Chem. Phys. **122**, 114103 (2005).

Baig, C., B. J. Edwards, D. J. Keffer, H. D. Cochran, and V. A. Harmandaris, "Rheological and structural studies of liquid polyethylenes under planar elongational flow using nonequilibrium molecular dynamics simulations," J. Chem. Phys. **124**, 084902 (2006).

Baig, C., V. G. Mavrantzas, and M. Kröger, "Flow effects on melt structure and entanglement network of linear polymers: Results from a nonequilibrium molecular dynamics simulation study of a polyethylene melt in steady shear," Macromolecules **43**, 6886–6902 (2010).

Bird, R. B., C. F. Curtiss, R. C. Armstrong, and O. Hassager, *Dynamics of Polymeric Liquids* (Wiley, New York, 1987a), Vol. II.

Bird, R. B., R. C. Armstrong, and O. Hassager, *Dynamics of Polymeric Liquids* (Wiley, New York, 1987b), Vol. I.

Dambal, A., A. Kushwaha, and E. S. G. Shaqfeh, "Slip-link simulations of entangled, finitely extensible, wormlike chains in shear flow," Macromolecules **42**, 7168–7183 (2009).

de Gennes, P. G., "Reptation of a polymer chain in the presence of fixed obstacles," J. Chem. Phys. **55**, 572–579 (1971).

Doi, M., and S. F. Edwards, *The Theory of Polymer Dynamics* (Clarendon, Oxford, 1986).

Doyle, P. S., E. S. G. Shaqfeh, and A. P. Gast, "Dynamic simulation of freely draining flexible polymers in steady linear flows," J. Fluid Mech. **334**, 251–291 (1997).

Edberg, R., G. P. Morriss, and D. J. Evans, "Rheology of *n*-alkanes by nonequilibrium molecular dynamics," J. Chem. Phys. **86**, 4555–4570 (1987).

Edwards, B. J., C. Baig, and D. J. Keffer, "An examination of the validity of nonequilibrium molecular-dynamics simulation algorithms for arbitrary steady-state flows," J. Chem. Phys. **123**, 114106 (2005).

Edwards, B. J., C. Baig, and D. J. Keffer, "A validation of the p-SLLOD equations of motion for homogeneous steady-state flows," J. Chem. Phys. **124**, 194104 (2006).

Edwards, B. J., and M. Dressler, "A reversible problem in non-equilibrium thermodynamics: Hamiltonian evolution equations for non-equilibrium molecular dynamics simulations," J. Non-Newtonian Fluid Mech. **96**, 163–175 (2001).

Evans, D. J., and G. P. Morriss, *Statistical Mechanics of Nonequilibrium Liquids* (Academic, London, 1990).

Everaers, R., "Topological versus rheological entanglement length in primitive-path analysis protocols, tube models, and slip-link models," Phys. Rev. E **86**, 022801 (2012).

Fetters, L. J., D. J. Lohse, and R. H. Colby, "Chain dimensions and entanglement spacings," in *Physical Properties of Polymers Handbook*, 2nd ed., edited by J. E. Mark (Springer, New York, 2007), chap. 25.

Fetters, L. J., D. J. Lohse, S. T. Milner, and W. W. Graessley, "Packing length influence in linear polymer melts on the entanglement, critical, and reptation molecular weights," Macromolecules **32**, 6847–6851 (1999).

Harasim, M., B. Wunderlich, O. Peleg, M. Kröger, and A. R. Bausch, "Direct observation of the dynamics of semiflexible polymers in shear flow," Phys. Rev. Lett. **110**, 108302 (2013).

Hoover, W. G., "Canonical dynamics: Equilibrium phase-space distributions," Phys. Rev. A **31**, 1695–1697 (1985).

Islam, M. T., J. Sanchez-Reyes, and L. A. Archer, "Step and steady shear responses of nearly monodisperse highly entangled 1,4-polybutadiene solutions," Rheol. Acta **42**, 191–198 (2003).

Karayiannis, N. Ch., and M. Kröger, "Combined molecular algorithms for the generation, equilibration and topological analysis of entangled polymers: methodology and performance," Int. J. Mol. Sci. **10**, 5054–5089 (2009).

Kim, J. M., B. J. Edwards, and D. J. Keffer, "Visualization of conformational changes of linear short-chain polyethylenes under shear and elongational flows," J. Mol. Graphics Modell. **26**, 1046–1056 (2008a).

Kim, J. M., B. J. Edwards, D. J. Keffer, and B. Khomami, "Single-chain dynamics of linear polyethylene liquids under shear flow," Phys. Lett. A **373**, 769–772 (2009).

Kim, J. M., B. J. Edwards, D. J. Keffer, and B. Khomami, "Dynamics of individual molecules of linear polyethylene liquids under shear: Atomistic simulation and comparison with a free-draining bead-rod chain," J. Rheol. **54**, 283–310 (2010).

Kim, J. M., D. J. Keffer, M. Kröger, and B. J. Edwards, "Rheological and entanglement characteristics of linear chain polyethylene liquids in planar Couette and planar elongational flows," J. Non-Newtonian Fluid Mech. **152**, 168–183 (2008b).

Kim, J. M., P. S. Stephanou, B. J. Edwards, and B. Khomami, "A Mean-field anisotropic diffusion model for unentangled polymeric liquids and semi-dilute solutions: model development and comparison with experimental and simulation data," J. Non-Newtonian Fluid Mech. **166**, 593–606 (2011).

Kröger, M., "Shortest multiple disconnected path for the analysis of entanglements in two- and three-dimensional polymeric systems," Comput. Phys. Commun. **168**, 209–232 (2005).

Kröger, M., and S. J. Hess, "Rheological evidence for a dynamical crossover in polymer melts via nonequilibrium molecular dynamics," Phys. Rev. Lett. **85**, 1128–1131 (2000).

Kröger, M., W. Loose, and S. J. Hess, "Rheology and structural changes of polymer melts via nonequilibrium molecular dynamics," J. Rheol. **37**, 1057–1079 (1993).

Kushwaha, A., and E. S. G. Shaqfeh, "Slip-link simulations of entangled polymers in planar extensional flow: Disentanglement modified extensional thinning," J. Rheol. **55**, 463–483 (2011).

Larson, R. G., *Constitutive Equations for Polymer Melts and Solutions* (Butterworths, Boston, 1988).

Larson, R. G., *The Structure and Rheology of Complex Fluids* (Oxford University, Oxford, 1999).

LeDuc, P., C. Haber, G. Bao, and D. Wirtz, "Dynamics of individual flexible polymers in a shear flow," Nature **399**, 564–566 (1999).

Liu, T. W., "Flexible polymer chain dynamics and rheological properties in steady flows," J. Chem. Phys. **90**, 5826–5842 (1989).

Mavrantzas, V. G., and D. N. Theodorou, "Atomistic simulation of polymer melt elasticity: calculation of the free energy of an oriented polymer melt," Macromolecules **31**, 6310–6332 (1998).

Mavrantzas, V. G., and H. C. Öttinger, "Atomistic Monte Carlo simulations of polymer melt elasticity: Their nonequilibrium thermodynamics GENERIC formulation in a generalized canonical ensemble," Macromolecules **35**, 960–975 (2002).

McLeish, T. C. B., "Tube theory of entangled polymer dynamics," Adv. Phys. **51**, 1379–1527 (2002).

Mhetar, V. R., and L. A. Archer, "A new proposal for polymer dynamics in steady shearing flows," J. Polym. Sci. B: Polym. Phys. **38**, 222–233 (2000).

Moore, J. D., S. T. Cui, H. D. Cochran, and P. T. Cummings, "A molecular dynamics study of a short-chain polyethylene melt. I. Steady-state shear," J. Non-Newtonian Fluid Mech. **93**, 83–99 (2000).

Nosé, S., "A molecular dynamics method for simulations in the canonical ensemble," Mol. Phys. **52**, 255–268 (1984).

Öttinger, H. C., *Stochastic Processes in Polymeric Fluids* (Springer, Berlin, 1996).

Robertson, R. M., and D. E. Smith, "Direct measurement of the intermolecular forces confining a single molecule in an entangled polymer solution," Phys. Rev. Lett. **99**, 126001 (2007).

Schieber, J., D. Nair, and T. Kitkrailard, "Comprehensive comparisons with nonlinear flow data of a consistently unconstrained Brownian slip-link model," J. Rheol. **51**, 1111–1141 (2007).

Schroeder, C. M., R. E. Teixeira, E. S. G. Shaqfeh, and S. Chu, "Characteristic periodic motion of a polymer in shear flow," Phys. Rev. Lett. **95**, 018301 (2005).

Shanbhag, S., and M. Kröger, "Primitive path networks generated by annealing and geometrical methods: insights into differences," Macromolecules **40**, 2897–2903 (2007).

Siepmann, J. I., S. Karaboni, and B. Smit, "Simulating the critical behavior of complex fluids," Nature **365**, 330–332 (1993).

Smith, D. E., and S. Chu, "Response of flexible polymers to a sudden elongational flow," Science **281**, 1335–1340 (1998).

Smith, D. E., H. P. Babcock, and S. Chu, "Single-polymer dynamics in steady shear flow," Science **283**, 1724–1727 (1999).

Somasi, M., B. Khomami, N. J. Woo, J. S. Hur, and E. S. G. Shaqfeh, "Brownian dynamics simulations of bead-rod and bead-spring chains: Numerical algorithms and coarse-graining issues," J. Non-Newtonian Fluid Mech. **108**, 227–255 (2002).

Stephanou, P. S., C. Baig, G. Tsolou,V. G. Mavrantzas, and M. Kröger, "Quantifying chain reptation in entangled polymer melts: topological and dynamical mapping of atomistic simulation results onto the tube model," J. Chem. Phys. **132**, 124904 (2010).

Teixeira, R. E., A. K. Dambal, D. H. Richter, E. S. G. Shaqfeh, and S. Chu, "The individualistic dynamics of entangled DNA in solution," Macromolecules **40**, 2461–2476 (2007).

Teixeira, R. E., H. P. Babcock, E. S. G. Shaqfeh, and S. Chu, "Shear thinning and tumbling dynamics of a single polymer in the flow-gradient plane," Macromolecules **38**, 581–592 (2005).

Travis, K. P., P. J. Daivis, and D. J. Evans, "Thermostats for molecular fluids undergoing shear flow: Application to liquid chlorine," J. Chem. Phys. **103**, 10638 (1995).

Venkataramani, V., R. Sureshkumar, and B. Khomami, "Coarse-grained modeling of macromolecular solutions using a configuration-based approach," J. Rheol. **52**, 1143–1177 (2008).